Prefrontal microglia deficiency during adolescence disrupts adult cognitive functions and synaptic structure: A follow-up study in female mice

von Arx, Anina S ; Dawson, Kara ; Lin, Han-Yu ; Mattei, Daniele ; Notter, Tina ; Meyer, Urs ; Schalbetter, Sina M

DOI: https://doi.org/10.1016/j.bbi.2023.04.007

Brain, Behavior, and Immunity 111 (2023) 230–246

Contents lists available at ScienceDirect

Brain Behavior and Immunity

journal homepage: www.elsevier.com/locate/ybrbi

Prefrontal microglia deficiency during adolescence disrupts adult cognitive functions and synaptic structures: A follow-up study in female mice

Anina S. von Arx [a], Kara Dawson [a], Han-Yu Lin [a], Daniele Mattei [b], Tina Notter [c,d], Urs Meyer [a,d,*], Sina M. Schalbetter [a]

[a] Institute of Veterinary Pharmacology and Toxicology, Vetsuisse, University of Zurich, Zurich, Switzerland
[b] MSSM Department of Neuroscience, Icahn School of Medicine at Mount Sinai, New York, NY, USA
[c] Institute of Pharmacology and Toxicology, University of Zurich, Zurich, Switzerland
[d] Neuroscience Center Zurich, University of Zurich and ETH Zurich, Zurich, Switzerland

ARTICLE INFO

Keywords:
Cognitive functions
Clodronate
Microglia depletion
Prefrontal cortex
Sensitive periods
Synaptic pruning
Schizophrenia

ABSTRACT

The prefrontal cortex (PFC) provides executive top-down control of a variety of cognitive processes. A distinctive feature of the PFC is its protracted structural and functional maturation throughout adolescence to early adulthood, which is necessary for acquiring mature cognitive abilities. Using a mouse model of cell-specific, transient and local depletion of microglia, which is based on intracerebral injection of clodronate disodium salt (CDS) into the PFC of adolescent male mice, we recently demonstrated that microglia contribute to the functional and structural maturation of the PFC in males. Because microglia biology and cortical maturation are partly sexually dimorphic, the main objective of the present study was to examine whether microglia similarly regulate this maturational process in female mice as well. Here, we show that a single, bilateral intra-PFC injection of CDS in adolescent (6-week-old) female mice induces a local and transient depletion (70 to 80% decrease from controls) of prefrontal microglia during a restricted window of adolescence without affecting neuronal or astrocytic cell populations. This transient microglia deficiency was sufficient to disrupt PFC-associated cognitive functions and synaptic structures at adult age. Inducing transient prefrontal microglia depletion in adult female mice did not cause these deficits, demonstrating that the adult PFC, unlike the adolescent PFC, is resilient to transient microglia deficiency in terms of lasting cognitive and synaptic maladaptations. Together with our previous findings in males, the present findings suggest that microglia contribute to the maturation of the female PFC in a similar way as to the prefrontal maturation occurring in males.

1. Introduction

The prefrontal cortex (PFC) is the cortical region covering the anterior part of the frontal lobe in the mammalian brain (Carlén, 2017). It provides executive top-down control of a variety of cognitive processes, including attention, working memory, decision making, and goal-directed behavior (Koechlin et al., 2003; Le Merre et al., 2021). The PFC also plays a key role in the development of personality and social functions (Bicks et al., 2015). Notably, dysfunction of the PFC is a central feature of many psychiatric disorders, especially of those that typically emerge during adolescence or early adulthood, such as schizophrenia and bipolar disorder (Sakurai et al., 2015; Selemon and Zecevic, 2015; Harrison et al., 2020).

A distinctive feature of the PFC is its protracted structural and functional maturation, which is sustained throughout adolescence until early adulthood (Caballero et al., 2016; Larsen and Luna, 2018; Chini and Hanganu-Opatz, 2021). Thus, the PFC is recognized as being one of the last brain regions to reach full maturity in humans (Gogtay et al., 2004) and in other species, including rodents (Chini and Hanganu-Opatz, 2021). The protracted maturation of the PFC is necessary for acquiring mature cognitive abilities and involves substantial refinement of neuronal circuitries and synaptic connections (Chini and Hanganu-Opatz, 2021). This refinement adapts prefrontal circuits to respond optimally to the changing demands occurring during the transition from adolescence to adulthood (Caballero et al., 2016; Larsen and Luna, 2018).

We have recently shown that microglia, the brain's resident immune cells, contribute to functional and structural maturation of the PFC

* Corresponding author at: Institute of Pharmacology and Toxicology Vetsuisse, University of Zurich, Winterthurerstrasse 260, 8057 Zurich, Switzerland.
E-mail address: urs.meyer@vetpharm.uzh.ch (U. Meyer).

https://doi.org/10.1016/j.bbi.2023.04.007
Received 8 November 2022; Received in revised form 30 March 2023; Accepted 23 April 2023
Available online 24 April 2023

(Schalbetter et al., 2022). Using a mouse model of cell-specific, transient and local depletion of microglia, we found that deficiency of prefrontal microglia during adolescence is sufficient to induce an adult emergence of PFC-associated impairments in cognitive functions, dendritic complexity, and synaptic structures and functions (Schalbetter et al., 2022). Intriguingly, there were no cognitive or synaptic sequelae when prefrontal microglia were depleted at adult age (Schalbetter et al., 2022). Hence, these data suggest that adolescence is a sensitive period for prefrontal microglia to act on PFC-related cognitive development and synaptic refinement, whereas the adult PFC is resilient to transient microglia deficiency in terms of possible behavioral and cognitive maladaptations (Schalbetter et al., 2022).

These findings were, however, based on investigations using male mice only (Schalbetter et al., 2022). Hence, it remains unknown whether microglia similarly regulate functional and structural maturation of the female PFC as well. Extending these investigations to the female sex is warranted for various reasons. First, there are marked sex differences in microglia biology in both health and disease (Schwarz and Bilbo, 2012; Hanamsagar et al., 2017; Guneykaya et al., 2018; VanRyzin et al., 2019), indicating that the influence of microglia on prefrontal maturation may be sexually dimorphic. Second, synaptic refinement within the PFC appears to follow sex-dependent temporal patterns, with adolescent synaptic pruning occurring earlier in females than males (Koss et al., 2014; Drzewiecki et al., 2016). Third, sex differences also exist with regards to the prevalence and clinical course of psychiatric disorders, including those that involve abnormal PFC functions (Riecher-Rössler, 2017; Chai et al., 2021; Ferrer-Quintero et al., 2022).

Therefore, the main objective of the present study was to investigate whether microglia contribute to the structural and functional maturation of the PFC in female mice. To achieve this goal, we implemented the same experimental approach previously used in males, which enabled us to manipulate microglia selectively in the PFC during a restricted time window of adolescence (Schalbetter et al., 2022). More specifically, we induced transient microglia deficiency by a single, bilateral stereotaxic injection of clodronate disodium salt (CDS) into the PFC of adolescent female mice. CDS induces apoptosis of microglia through inhibition of their mitochondrial adenosine 5′-diphosphate/adenosine 5′-triphosphate (ATP) translocase (Lehenkari et al., 2002; Torres et al., 2016). As previously demonstrated, intra-PFC injection of CDS in 6-week-old male mice is a potent and highly selective method to induce a local and transient depletion of prefrontal microglia during adolescence, which does not induce non-specific effects on other cells of the central nervous system (CNS) or peripheral immune cell infiltration (Schalbetter et al., 2022).

Here, we used this model to examine whether behavioral and cognitive development of female mice is influenced by prefrontal microglia deficiency during adolescence. To this aim, female mice were subjected to intra-PFC CDS or control injections during adolescence, after which they were allowed to mature until adulthood. Adult behavioral and cognitive testing encompassed tests that critically depend on PFC functions, including social approach behavior and social recognition memory (Bicks et al., 2015), temporal order memory (Barker et al., 2007), and extinction of contextual fear memory (Sotres-Bayon et al., 2006; Maren et al., 2013). We also investigated whether transient prefrontal microglia depletion during adolescence alters the density of excitatory and inhibitory synapses in the adult PFC of female mice. Finally, to explore whether adolescence is a window of increased vulnerability for cognitive and synaptic sequelae after transient microglia deficiency (Schalbetter et al., 2022), we applied the same microglia-depleting manipulation to adult female mice and examined possible effects on behavior, cognition and synaptic structures.

2. Materials and methods

2.1. Animals

All experiments were performed using female C57BL6/N mice (Charles Rivers, Sulzfeld, Germany). The animals were kept in groups (2–5 animals per cage) in individually ventilated cages (Allentown Inc., Bussy-Saint- Georges, France) in a temperature- and humidity-controlled (21 ± 3 °C, 50 ± 10%) specific-pathogen-free (SPF) holding room. They were kept under a reversed light–dark cycle (lights off: 09:00 AM–09.00 PM) and had *ad libitum* access to standard rodent chow (Kliba 3336, Kaiseraugst, Switzerland) and water throughout the entire study. All experiments were previously approved by the Cantonal Veterinarian's Office of Zurich, Switzerland (license nr. ZH-187/2017). All efforts were made to minimize the number of animals used and their suffering.

2.2. Stereotaxic surgery

A schematic overview of the main experimental design of this study is provided in Fig. 1. The stereotaxic surgery was performed using methods established and validated before (Schalbetter et al., 2021, 2022). Anesthesia was induced by inhalation of 4% isoflurane (ZDG9623V, Baxter, Switzerland) in oxygen. After anesthesia induction, the heads of the animals were shaved, and vitamin A cream (Bausch & Lomb Swiss AG) was applied to the eyes to avoid dehydration. The animals were injected with the analgesic (Temgesic buprenorphine [0.1 mg/kg, s.c.], Reckitt Benckiser, Switzerland) and fixed into the stereotaxic frame (MTM-3, World Precision Instruments, USA) while kept under constant isoflurane/oxygen flow (1 to 3% isoflurane in oxygen at 600 ml/min). All animals were kept on a temperature-controlled heating plate (ATC1000, World Precision Instruments, USA) during the entire surgical procedure to avoid anesthesia-induced hypothermia. A longitudinal incision of the skin was made to expose the skull. The skull was cleaned from connective tissue, and the bone, above the target area, was removed using a micro drill (OmniDrill35, World Precision Instruments, USA) with a rose burr (ø 0.3 mm). Intracerebral injections were performed using a NanoFil needle and syringe (NANOFIL, NF35BV, World Precision Instruments, USA) connected to an automated pump (UMP3T-1, World Precision Instruments, USA).

Mice assigned to transient prefrontal microglia depletion received a single, bilateral injection of CDS (50 mg/ml in PBS; catalog no. 233183, EMD Millipore Corp., USA) into the medial portion of the PFC, whereas control mice received a single, bilateral injection of phosphate buffered saline (PBS; catalog no. 14190144, Thermo Fisher Scientific, Switzerland). The solutions were injected at an infusion rate of 5 nl/s and a volume of 200 nl (6-week-old mice) or 300 nl (12-week-old mice). Bilateral injections were performed at defined stereotaxic coordinates of the PFC with reference to bregma. For adolescent (6-week-old) mice, the following coordinates were used: anteroposterior (A/P) = $^{+}$1.80 mm, mediolateral (M/L) = ±0.3 mm, and dorsoventral (D/V) = −1.90 mm; for adult (12-week-old) mice, the following coordinates were used: A/P = $^{+}$2.0 mm, M/L = ±0.3 mm, and D/V = −2.0 mm. After insertion of the needle, a small drop of Histoacryl (B. Braun, Switzerland) was applied at the site of injection to avoid reflux of the injected substances. After injection of either PBS or CDS, the needle was kept in place for 5 min to avoid reflux of the substances before retracting it. For some experiments, an additional group of animals was fixed into the stereotaxic frame and had a longitudinal incision made but were otherwise left undisturbed. These mice served as additional sham controls. Incisions were sutured with a surgical thread (G0932078, B. Braun, Switzerland), and the animals were placed in a temperature-controlled chamber (Harvard Apparatus, USA) until full recovery from anesthesia. After the surgery, the animals were placed back in their home cage and closely monitored for three consecutive days after surgery.

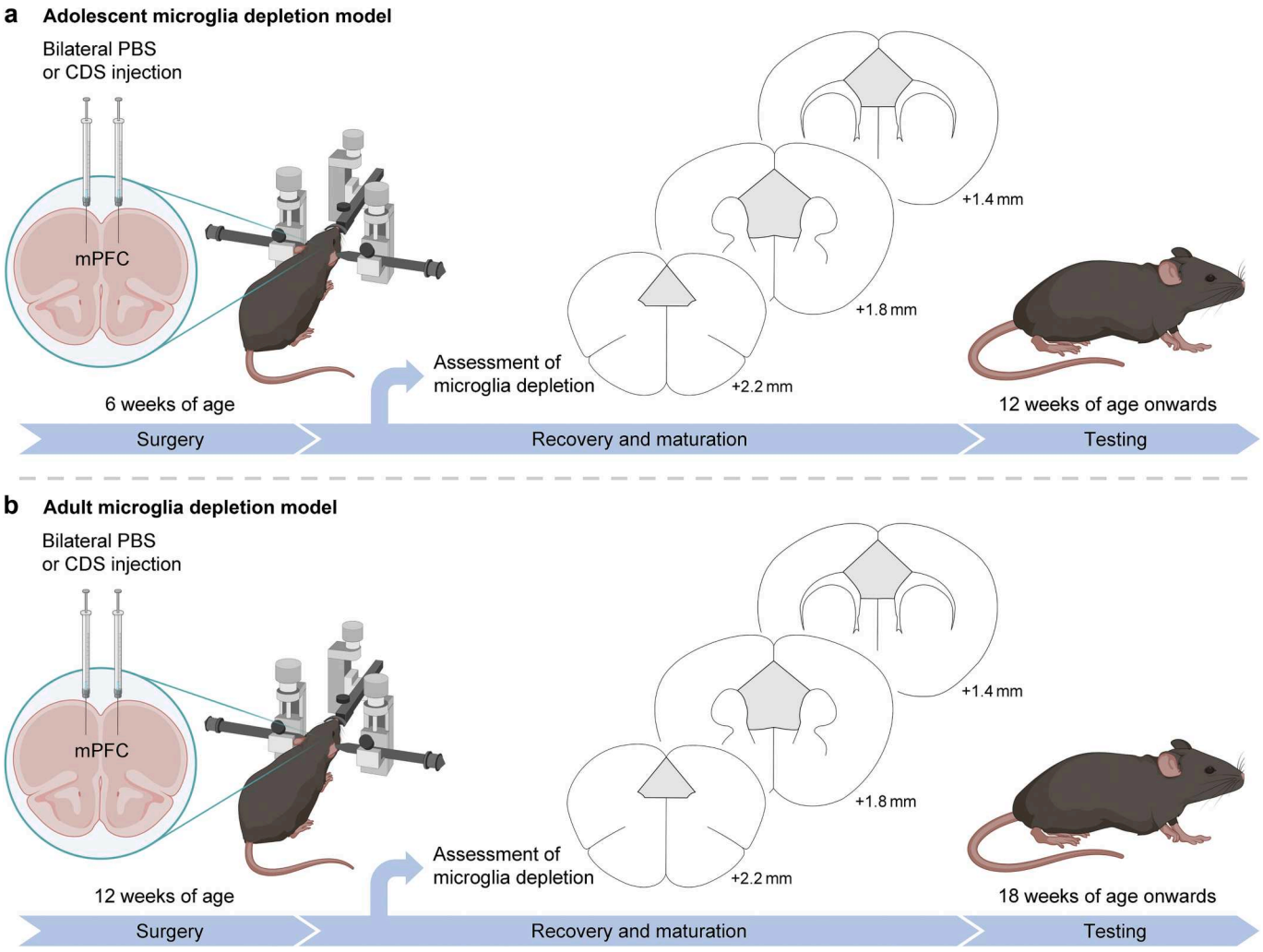

Fig. 1. Main experimental design of the study. (a) To deplete microglia selectively and transiently from the prefrontal cortex (PFC) during a defined window of adolescence, 6-week-old C57BL6/N female mice received a single, bilateral stereotaxic injection of clodronate disodium salt (CDS) into the medial PFC (mPFC). Control mice received a bilateral stereotaxic injection of phosphate-buffered saline (PBS). A group of mice receiving sham surgery, which involved the same surgical procedures but no stereotaxic injections, was included as an additional, negative control group for some experiments (not depicted in the figure). The magnitude and specificity of microglia depletion were ascertained by post-mortem immunohistochemistry in the mPFC (as highlighted by the gray area in the schematic coronal sections) along the anterior (bregma + 2.2. mm) to posterior (bregma + 1.4 mm) axis, which was conducted at successive time points (1, 5, 10, and 20 days post-injection [dpi]) after CDS or PBS injection or sham surgery. Additional morphological analyses of repopulated microglia were conducted at 10, 20 and 40 dpi. To test the effects of adolescent microglia depletion on adult behavioral and cognitive functions and synaptic densities, 6-week-old C57BL6/N female mice received a single, bilateral stereotaxic injection of CDS or PBS into mPFC and were then allowed to recover and mature into adulthood. Adult testing commenced at 12 weeks of age. (b) To deplete microglia selectively and transiently from the PFC in adulthood, 12-week-old C57BL6/N female mice received a single, bilateral stereotaxic injection of CDS into the mPFC. Control mice received a bilateral stereotaxic injection of PBS. The magnitude and specificity of microglia depletion were ascertained by post-mortem immunohistochemistry in the mPFC (as highlighted by the gray area in the schematic coronal sections) at 5 and 20 days post-injection (dpi) along the anterior (bregma + 2.2. mm) to posterior (bregma + 1.4 mm) axis. The 5 dpi interval was selected to capture the peak of CDS-induced microglia depletion, whereas the 20 dpi interval was chosen to ascertain the full restoration of the prefrontal microglia population after transient depletion in adulthood. To examine possible effects of adult microglia depletion on behavioral and cognitive functions and synaptic densities, 12-week-old C57BL6/N female mice were injected with either CDS or PBS and were allowed to recover for 6 weeks. A recovery period of 6 weeks was chosen to match the recovery and maturation period used in experiments, in which microglia were transiently depleted from the PFC of adolescent mice. Hence, in the adult microglia depletion model, behavioral and cognitive functions and synaptic densities were assessed starting at 18 weeks of age.

2.3. Behavioral and cognitive testing

Behavioral and cognitive testing involved a battery of tests indexing basal locomotor activity and innate anxiety-like behavior (open field test and light–dark box test), social approach behavior and recognition memory (social interaction test), temporal order memory for objects (temporal order memory test) and contextual fear conditioning and extinction (fear conditioning test). The tests for social approach behavior and recognition memory, temporal order memory, and contextual fear conditioning and extinction were selected because they critically involve PFC functions (Sotres-Bayon et al., 2006; Barker et al., 2007; Maren et al., 2013; Bicks et al., 2015). Tests for basal locomotor activity and innate anxiety-like behavior were conducted to evaluate whether the anticipated changes in PFC-related cognitive functions after microglia depletion would be confounded by possible alterations in general exploratory activity or innate anxiety-like behavior. In each experimental series, the animals were tested repeatedly using the same order of testing (1. open field test; 2. light–dark box test; 3. social interaction test; 4. temporal order memory test, 5. fear conditioning test), with a resting phase of 3–4 days between individual tests. Testing

was always conducted during the animals' active phase, that is, during the dark phase of the inverted light–dark cycle (between 10:00 AM–08.00 PM). All tests were extensively validated before (Labouesse et al., 2015; Richetto et al., 2015; Weber-Stadlbauer et al., 2017; Mueller et al., 2021; Schalbetter et al., 2022).

2.3.1. Open field test

A standard open field exploration task served as a first test to assess spontaneous locomotor activity and innate anxiety-like behavior (Belzung and Griebel, 2001). The apparatus consisted of four identical open field arenas (40 [length] × 40 [width] × 35 [height] cm) made of white polyvinyl chloride (OCB Systems Ltd., Hertfordshire, UK). It was positioned in a testing room with diffused lighting (~30 lx in center of the arena). A digital camera was mounted above the arena, captured images at a rate of 5 Hz and transmitted them to a PC running the EthoVision (Noldus Technology, Wageningen, The Netherlands) tracking system. The animals were recorded for 15 min before they were placed back into their home cage. For the purpose of data collection, the arena was conceptually partitioned into two areas: a center zone (measuring 10 × 10 cm) in the middle of the area, and a peripheral zone occupying the remaining area. The measurements collected from this test included the total distance moved, the distance moved in the center zone, and the number of center zone visits. The total times spent rearing and grooming were also measured and analyzed as additional measures of exploratory behavior.

2.3.2. Light-dark box test

A light–dark box test was used as a second test to measure innate anxiety-like behavior (Belzung and Griebel, 2001). The apparatus consisted of 4 identical multi-conditioning boxes (Multi Conditioning System, TSE Systems, Bad Homburg, Germany), each containing a dark (1 lx) and a bright (100 lx) compartment. The two compartments were separated from each other by a dark plexiglass wall with an integrated, electrically controlled door. To start a trial, each mouse was placed in the dark compartment. After 5 s the door automatically opened, allowing access to both the dark and bright compartment for 10 min. The measurements collected from this test included the distance moved and time spent in the light compartment.

2.3.3. Social approach and social recognition memory test

Social approach behavior and social recognition memory were measured using a social interaction test consisting of two phases (Richetto et al., 2015; Weber-Stadlbauer et al., 2017). The apparatus was made of a modified Y-maze consisting of opaque acrylic glass, which contained three identical arms (50 [length] × 9 [width] cm) surrounded by 10-cm high Plexiglas walls. The three arms radiated from a central triangle (8 cm on each side) and were spaced 120° from each other. Two of the three arms contained rectangular wire grid cages (13 [length] × 8 [width] × 10 [height] cm), with metal bars horizontally and vertically spaced 9 mm apart. The third arm did not contain a metal wire cage and served as the start zone (see below). The apparatus was located in an experimental testing room under dim diffused lighting (~20 lx as measured in the individual arms).

Phase 1: This phase served as a test for social approach behavior. During this phase, one metal wire cage contained an unfamiliar C57BL6/N mouse ('live mouse'), whereas the other wire cage contained an inanimate object ('dummy object'). The latter was a black scrunchie made of velvet material. The allocation of the 'live mouse' and 'dummy' to the two wire cages was counterbalanced across experimental groups. To begin a trial, the test animal was introduced at the end of the start arm and was allowed to freely explore all three arms for 5 min. Behavioral observations were made by an experimenter who was blinded to the experimental conditions in the form of numerical codes. Social interaction was defined as nose contact within a 2-cm interaction zone. For each test animal, a social preference index was calculated by the formula: ([time spent with the mouse] / [time spent with the inanimate dummy object $^{+}$ time spent with the mouse]) − 0.5. The social preference index was used to compare the relative exploration time between the unfamiliar mouse and the inanimate dummy object, with values > 0 signifying a preference toward the unfamiliar mouse. In addition, the absolute times spent with the unfamiliar mouse and the inanimate dummy object were analyzed. On completion of phase 1, the animal was removed and kept in a holding cage for 5 min until the start of the next phase.

Phase 2: This phase served as a test for social recognition memory. During this phase, another unfamiliar C57BL6/N mouse, which is referred to as the 'novel mouse', replaced the inanimate dummy object. The other cage contained the 'familiar mouse' previously used in phase 1 (see above) of the test. The allocation of the 'novel mouse' and 'familiar mouse' to the two wire cages was counterbalanced across experimental groups. To start phase 2, the test animal was introduced at the end of the start arm and was allowed to freely explore all three arms for 5 min. Behavioral observations for social interaction were scored as described before. For each test animal, a social memory index was calculated by the formula: ([time spent with the novel mouse] / [time spent with the novel mouse $^{+}$ time spent with the familiar mouse]) − 0.5. The social memory index was used to compare the relative exploration time between the familiar and novel mouse, with values > 0 signifying a preference toward the novel mouse. In addition, the absolute times spent with the familiar and novel mouse were analyzed.

2.3.4. Temporal order memory test

A temporal order memory test for objects was used to measure the PFC-dependent capacity of animals to discriminate the relative recency of stimuli (Barker et al., 2007). The test apparatus consisted of an open field as described above, with minor modifications (see below). The test procedure consisted of 4 consecutive phases, which were each separated 60 min apart.

Habituation phase: To habituate the animals to the test apparatus, the animals were gently placed in the center of the open field apparatus and allowed to freely explore the arena for 10 min. They were then removed from the apparatus and kept in a holding room for 60 min before the start of the next phase.

Sample phase 1: For this phase, a first pair of identical objects (blue aluminum hairspray bottles, 250 ml, 20 cm high) were placed in the open field arena in opposing corners approximately 5 cm from the walls. To start a trial, the animals were gently placed into the center of the open field and were allowed to freely explore the objects for 10 min. They were then removed from the apparatus again and kept in a holding room for 60 min before the start of the next phase.

Sample phase 2: For this phase, a novel pair of identical objects (LEGO® Duplo brick pile, 15 cm high) were placed in the open field arena, thereby allocating them in the same position as the first pair of objects (see above). To start a trial, the animals were gently placed into the center of the open field again and were allowed to freely explore the novel pair of objects for 10 min. They were then removed from the apparatus once more and kept in a holding room for 60 min before the start of the actual test phase.

Test phase: In the test phase, the open field was equipped with one object used in sample phase 1 (temporally more remote object), and one object in sample phase 2 (temporally more recent object), with the corner allocation of the objects being counterbalanced across groups. To start the test trial, the animals were placed into the center of the open field and were allowed to freely explore either object for 10 min.

For each animal, a temporal order memory index was calculated by the formula: ([time spent with phase 1 object] / [time spent with phase 1 object $^{+}$ time spent with phase 2 object]) − 0.5. The temporal order memory index was used to compare the animals' capacity to discriminate the relative recency of stimuli (Barker et al., 2007), with values > 0 signifying a capacity to discriminate between the temporally more remote object presented in sample phase 1 and the temporally more recent object presented in sample phase 2. In addition, the relative

amount of time exploring the objects in sample phases 1 and 2 of the test were analyzed to measure object exploration per se and to explore possible side preferences while exploring the objects.

2.3.5. Contextual fear conditioning and extinction test

Contextual fear conditioning and extinction were conducted using 4 identical multi-conditioning chambers (Multi Conditioning System, TSE Systems, Bad Homburg, Germany), in which the animals were confined to a rectangular enclosure (30 [length] × 30 [width] × 36 [height] cm) made of black acrylic glass. The chambers were equivalently illuminated by a red house light (30 lx) and were equipped with a grid floor made of 29 stainless rods (4 mm in diameter and 10 mm apart; inter-rod center to inter-rod center), through which a scrambled electric shock could be delivered. Each chamber was surrounded by 3 infrared light-beam sensor systems, with sensors spaced 14 mm apart, allowing movement detection in 3 dimensions. The contextual fear conditioning and extinction test followed protocols established before (Labouesse et al., 2015) and consisted of 3 phases, which were each separated 24 h apart (see below). During all three phases, the red house light was on at all times. Conditioned fear was expressed as freezing behavior, which was quantified automatically by program-guided algorithms as time of immobility per 30-sec bins. The data collected during the three phases were analyzed separately.

Habituation and conditioning phase: The animals were placed in the designated test chamber and were allowed to freely explore the chamber for 3 min. This served to habituate the animals to the chamber. Conditioning commenced immediately at the end of the habituation period without the animals being removed from the chambers. For conditioning, the animals were exposed to 3 conditioning trials, whereby each conditioning trial began with the delivery of a 1-s foot-shock set at 0.3 mA and was followed by a 90 s rest period. After the last conditioning trial, the animals were removed from the chambers and were placed back in their home cages. The amount of percent time freezing during each post-shock period was divided into bins of 30 s and provided a measure of the contextual fear acquisition.

Fear expression phase: The fear expression phase took place 24 h after conditioning when the animals were returned to the same chambers in the absence of any discrete stimulus other than the context. To assess conditioned fear toward to the context, percent time freezing was measured for a period of 6 min and expressed as a function of 30-s bins. The animals were then removed from the boxes and placed back to their home cages.

Fear extinction phase: Extinction of contextual fear memory was evaluated by daily exposing the animals to the same chambers in the absence of any discrete stimulus other than the context (Sotres-Bayon et al., 2006; Maren et al., 2013). This procedure was conducted on three consecutive days, during which the animals were exposed to the chamber for a total of 6 min on each day. To analyze extinction of contextual fear memory, the extinction rate was calculated for each animal by expressing the percent time freezing measured on each day of the fear extinction phase relative to baseline percent time freezing measured during the fear expression phase 24 h after conditioning.

2.4. Immunohistochemistry

The animals were deeply anesthetized with an overdose of pentobarbital (Esconarkon ad us. vet., Streuli Pharma AG, Switzerland) and transcardially perfused with 20 ml of ice-cold PBS followed by 60 ml of ice-cold 4% phosphate-buffered paraformaldehyde (PFA) with a perfusion rate of 20 ml/min. The brains were immediately removed from the skull and post-fixed in 4% PFA for 6 h before cryoprotection in 30% sucrose in PBS for 48 h. The brains were cut coronally with a sliding microtome at 30 μm (8 serial sections) and stored at − 20 °C in cryoprotectant solution (50 mM sodium phosphate buffer (pH 7.4) containing 15% glucose and 30% ethylene glycol; Sigma-Aldrich, Switzerland) until further processing.

Immunofluorescent stainings were performed according to previously established protocols (Notter et al., 2014, 2018, 2021; Schalbetter et al., 2021, 2022). In brief, the brain sections were rinsed in Tris buffer (pH 7.4) before incubated with primary antibodies. A summary of all antibodies used for the immunohistochemical experiments are provided in Table 1 (primary antibodies) and Table 2 (secondary antibodies). The primary antibodies were diluted in Tris buffer containing 0.2% Triton X-100 and 2% normal serum. The sections were incubated free-floating under constant agitation (100 rpm) overnight at 4 °C. The following day, sections were washed 3 × 10 min in Tris buffer prior to a 30 min incubation period with secondary antibodies diluted in Tris buffer containing 2% normal serum at room temperature. After incubation, which was shielded from light, the sections were washed 3 × 10 min in Tris buffer, mounted onto gelatinized glass slides, coverslipped with Dako fluorescence mounting medium (S3023, Agilent, Switzerland), and stored in the dark at 4 °C until image acquisition (see below).

2.5. Microscopy and immunofluorescent image analyses

2.5.1. Assessment of cell numbers

Immunofluorescence (IF)-stained images of Iba1$^+$ microglia, NeuN$^+$ neurons and S100β$^+$ astrocytes were acquired with a widefield microscope (AxioObserver Z1, Zeiss, Jena, Germany) using a 10× (air, NA 0.3) objective. Consecutive tile-scans of whole coronal brain sections were captured (bregma: $^+$2.2 mm, $^+$1.8 mm, $^+$1.4 mm, and $^+$0.5 mm) and exported from the ZEN-Software as *tiff* format. Cell numbers within the region of interest (medial PFC, primary motor cortex, secondary motor cortex, primary somatosensory cortex, and forceps minor of the corpus callosum) were counted using the particle analyzer plugin for the ImageJ software. The threshold for each marker was set to acquire optimal representation of microglia, neurons, and astrocytes and kept constant during image analyses. Microglia, neuron and astrocyte cell numbers were normalized to each individual area of interest and displayed as cells/mm^2. All analyses were conducted by an experimenter who was blinded to the treatment conditions in form of numerical codes.

2.5.2. Analysis of microglia morphology and Sholl analysis

Immunofluorescent images of Iba1$^+$ microglia were taken by confocal laser scanning microscopy (Spinning disk, Visitron CSU-W1,

Table 1
List of primary antibodies used for immunohistochemistry.

Target	Vendor	Description, Cat#	Dilution
Gephyrin	Synaptic Systems, Germany	Mouse monoclonal, 147 011	1:1′000
Ionized calcium-binding adaptor molecule 1 (Iba1)	FUJIFILM Wako Chemicals, USA	Rabbit polyclonal, 019–19741	1:3′000
Neuronal nuclei (NeuN)	Synaptic Systems, Germany	Guinea pig polyclonal, 266 004	1:1′000
Postsynaptic density protein 95 (PSD-95)	Thermo Fisher Scientific, Switzerland	Rabbit polyclonal, 51–6900	1:1′000
S100 calcium-binding protein β (S100β)	Abcam, Netherlands	Rabbit monoclonal, ab52642	1:1′000
Vesicular glutamate transporter 1 (VGLUT1)	Synaptic Systems, Germany	Guinea pig polyclonal, 135 304	1:1′000
Vesicular inhibitory amino acid transporter (VGAT)	Synaptic Systems, Germany	Rabbit polyclonal, 131 002	1:1′000

The table specifies the vendor, description, catalogue number (Cat#) and dilution of the primary antibodies used for immunohistochemistry. The selected antibodies have been validated thoroughly in previous studies using C57BL6/N mice (Notter et al., 2014, 2018, 2021; Schalbetter et al., 2021, 2022).

Table 2
List of secondary antibodies used for immunohistochemistry.

Host species	Target species	Conjugate	Vendor	Cat#	Dilution
Goat	Rabbit	Alexa 488	Thermo Fisher Scientific, Switzerland	A-11008	1:500
Goat	Guinea pig	Cy3	Jackson ImmunoResearch Laboratories, Europe Ltd	106–165-003	1:500
Donkey	Rabbit	Alexa 488	Jackson ImmunoResearch Laboratories, Europe Ltd	711–545-152	1:500
Donkey	Guinea pig	Cy5	Jackson ImmunoResearch Laboratories, Europe Ltd	706–175-148	1:500
Donkey	Mouse	Cy3	Jackson ImmunoResearch Laboratories, Europe Ltd	715–165-150	1:500

The table specifies the host species, target species, conjugate, vendor, catalogue number (Cat#) and dilution of the secondary antibodies used for immunohistochemistry.

Visitron Systems, Puchheim, Germany) with a 100× (oil, NA 1.4) objective. The laser intensity for the channel was set and kept constant during the entire image acquisition. For each animal, 8 series of images with a minimal z-stack distance of 0.14 µm were randomly acquired from three consecutive sections containing the medial portion of the PFC spanning the infralimbic (IL), prelimbic (PL) and anterior cingulate (AC) subregions (bregma: +2.2 to + 1.4 mm). The images were imported into Imaris image analysis software (version 9.6.0, Oxford Instruments) and processed using a median filter. Iba1$^+$ microglial cells were reconstructed three-dimensionally using the "filament creation" wizard. Manual error correction was performed to ensure accurate microglial process rendering. The total number of branch points was quantified automatically by the software. For Sholl analysis, a sphere radius gap of 5 µm was chosen, and the number of microglial processes intersecting against the radial distance from soma was quantified automatically by the software.

The cell soma area of microglial cells was assessed using the ImageJ software, whereby confocal images of the z-stack were merged to a single image. For each cell, the soma area was drawn manually and measured automatically by the software.

On average, 10 randomly selected microglia per animal and dpi were included in the morphological and Sholl analyses, yielding a total of 50 microglia from $n = 5$ animal in each treatment group and dpi. To avoid spurious findings arising from pseudoreplication, the number of animals (rather than the number of cells) was considered as the experimental unit in all statistical analyses of microglia morphology and Sholl analysis.

2.5.3. Estimation of synaptic density via co-localization analysis

Double-IF images of VGLUT1 and PSD-95 (excitatory synapses) or VGAT and Gephyrin (inhibitory synapses) were taken using sequential acquisition of separate wavelength channels by confocal laser scanning microscopy (Leica DMI6000 AFC, Model SP8, Mannheim, Germany) with a 63× (oil, NA 1.4) objective and a zoom of 1.8. Laser intensities for each channel were set and kept constant during the entire image acquisition. For each animal, 6 single plane images were acquired for each subregion of the PFC (IL, PL and AC), from 3 consecutive sections (bregma: +2.2 mm to + 1.4 mm). Co-localization between VGLUT1$^+$ and PSD-95$^+$ puncta (excitatory synapses) or VGAT and Gephyrin (inhibitory synapses) were measured and calculated using a custom-made macro (kindly provided by Prof. emeritus Jean-Marc Fritschy, Institute of Pharmacology and Toxicology, University of Zurich, Switzerland) developed for the ImageJ software. This macro has been extensively validated for immunohistochemical co-localization studies and has been described in detail previously (Notter et al., 2018, 2021; Schalbetter et al., 2022). In brief, Gaussian filter, background subtraction and a threshold were applied to the images for each channel. The settings for each marker were adjusted so that an optimal representation of VGLUT1, PSD-95, VGAT and Gephyrin was achieved and kept constant during image analyses. The number of co-localized clusters was defined as pixel clusters in the presynaptic channel (VGLUT1 or VGAT) that overlapped with pixel clusters in the post-synaptic channel (PSD-95 or Gephyrin), with a set size cut-off at 0.05 µm^2.

2.6. Magnetic-activated cell sorting for microglia isolation

To quantify microglia-defining genes (*Csf1r*, *Cx3cr1*, *Iba1*, *P2ry12*, *P2ry6*, *Pu.1*, and *Trem2*; Wolf et al., 2017; Paolicelli et al., 2022) in microglial cell populations, microglia were isolated from the PFC using magnetic-activated cell sorting (MACS) of cells that were harvested using an optimized mechanical dissociation protocol at 4 °C as validated and described previously (Mattei et al., 2020). In brief, mice were deeply anesthetized with an overdose of pentobarbital (Esconarkon ad us. vet., Streuli Pharma AG, Switzerland) and transcardially perfused with 15 ml ice-cold, calcium- and magnesium-free Dulbecco's phosphate-buffered saline (DPBS, 14190144, Thermo Fisher Scientific, Switzerland) via a 20 ml syringe and a 23 G needle (25 mm length). The brains were quickly removed and washed with ice-cold DPBS, after which the PFC was dissected on a cooled petri dish and placed in an ice-cold Hibernate-A medium (HAPR, Brainbits). Mechanical dissociation was carried out on ice, while all the solutions were kept at 4 °C. The PFC samples of 3 mice were pooled per data point and were dissociated in 1.5 ml Hibernate-A medium in a 1 ml Dounce homogenizer (40401, Active Motif) with a loose pestle. The tissue was gently homogenized and then sieved through a 70 µm cell strainer (15370801, Fisher Scientific) mounted onto a 50 ml Falcon tube. The Dounce homogenizer was washed twice with 1 ml Hibernate-A, whereby each wash was poured onto the cell strainer. The homogenized PFC samples were then transferred to 5 ml Eppendorf tubes and kept on ice. The homogenates were pelleted at 400 × *g* for 6 min at 4 °C in a swing-bucket rotor centrifuge (Eppendorf, Schönenbuch, Switzerland). The supernatants were removed and 1 ml ice-cold DPBS was added to all samples. The pellets were then re-suspended with a P1000 micropipette. After re-suspension, the final volume in each tube was brought to 1.5 ml. 500 µl of freshly prepared isotonic percoll solution (17089101, GE Healthcare) was added to each sample and mixed well. Percoll was rendered isotonic by mixing 1 part of 10 × calcium- and magnesium-free DPBS (14200075, Thermo Fisher Scientific, Switzerland) with 9-parts of percoll. The pH of percoll was adjusted to 7.3–7.4 with 5 M hydrochloric acid before starting the isolation procedure. The percoll solution was mixed properly with the cell suspension, after which 2 ml of DPBS were gently layered on top of it, creating two separate layers. The samples were centrifuged for 10 min at 3000 × *g*. The centrifugation resulted in an upper layer consisting of DPBS and a lower layer consisting of percoll. The two layers were separated by a disk of myelin and debris, while the cells were located at the bottom of the tube. The layers above the cell pellet were aspirated leaving about 500 µl. The cells were then washed once in 4 ml DPBS making sure not to resuspend the pellet. The cells were then pelleted by centrifugation at 400 × *g* for 10 min at 4 °C.

Microglia were isolated by MACS using mouse anti-CD11b magnetic microbeads (130–093-634, Miltenyi) according to the manufacturer's instructions with some modifications. The MACS buffer used consisted of 1.5% bovine serum albumin (BSA) diluted in DPBS from a commercial 7.5% cell-culture grade BSA stock (Thermo Fisher Scientific, 11500496). For the isolation of microglia, cell pellets were re-suspended in 80 µl MACS buffer and 10 µl FcR-blocking reagent (Miltenyi). The cells were

then incubated for 10 min at 4 °C. Thereafter, 10 µl of anti-CD11b magnetic microbeads were added and the cells were incubated for 15 min at 4 °C. The cells were then washed with 1 ml MACS buffer and pelleted at 300 × *g* for 5 min at 4 °C. The cells were passed through an MS MACS column (130–042-201, Miltenyi) attached to a magnet. This led CD11b-labeled cells to stay attached to the column, whereas unlabeled cells flowed through. After washing the columns three times with MACS buffer, the columns were removed from the magnet and microglia were eluted with 1 ml MACS buffer and pelleted at 300 × g for 5 min at 4 °C.

Total RNA from the cell pellets was isolated using the SPLIT RNA Extraction Kit (008.48, Lexogen, Vienna, Austria). The procedure was conducted according to the manufacturer's instructions, and the resulting RNA was quantified by Nanodrop (DeNovix DS-11 + Spectrophotometer, Labgene Scientific SA, Switzerland). The samples were stored at −80 °C until further use (gene expression analyses using quantitative real-time polymerase chain reaction, see below).

2.7. Quantitative real-time polymerase chain reaction

Quantitative real-time polymerase chain reaction (qRT-PCR) was performed according to previously established protocols (Richetto et al., 2015; Notter et al., 2021; Schalbetter et al., 2021, 2022). RNA was extracted from microglial cells isolated via MACS as described above and was analyzed by TaqMan qRT-PCR instrument (CFX384 real-time system, Bio-Rad Laboratories) using the iScript one-step qRT-PCR kit for probes (Bio-Rad Laboratories). The samples were run in 384-well formats in triplicates as multiplexed reactions with a normalizing internal control (36B4). Thermal cycling was initiated with an incubation at 50 °C for 10 min (RNA retrotranscription) and then at 95 °C for 5 min (TaqMan polymerase activation). After this initial step, 39 cycles of PCR were performed. Each PCR cycle consisted of heating the samples at 95 °C for 10 s to enable the melting process, and then for 30 s at 60 °C for the annealing and extension reaction. Relative target gene expression was calculated according to the $2^{(\text{-Delta C(T)})}$ method (Livak and Schmittgen, 2001). Custom-designed probe and primer sequence used for the reference gene (36B4) and TaqMan assay ID's for the genes of interest are summarized in Table 3.

2.8. Statistical analyses

All statistical analyses were performed using SPSS Statistics (version 25.0, IBM, Armonk, NY, USA) and Prism (version 9.0; GraphPad Software, La Jolla, California), with statistical significance set at $p < 0.05$ unless specified otherwise. All data were acquired and analyzed in a blind manner, in which the treatment conditions were blinded in the form of numerical codes.

All immunohistochemical data involving 3 treatment groups (sham, PBS and CDS) were analyzed using one-way analysis of variance (ANOVA), followed by Tukey's post-hoc test for multiple comparisons. All immunohistochemical data involving 2 treatment groups (PBS and CDS) were analyzed using independent Student's *t*-tests (two-tailed), with the exception of the Sholl analysis data, which were analyzed using 2 × 12 (treatment × distance intervals) repeated-measures ANOVA, followed by Bonferroni post-hoc tests for multiple comparisons at individual distance intervals. All dependent variables in the open field test (total distance moved, distance moved in the center zone and number of center zone visits) and light–dark box test (total distance and time spent in the light compartment) were analyzed using independent Student's *t*-tests (two-tailed). In the social interaction test, the social preference index and social memory index were also analyzed using independent Student's *t*-tests (two-tailed), whereas the absolute times exploring the live mouse versus inanimate dummy object (phase 1), or the absolute times exploring the unfamiliar versus familiar mouse (phase 2), were analyzed using 2 × 2 (treatment × object) repeated-measures ANOVA, followed by repeated-measures ANOVA restricted to either treatment group (PBS or CDS) whenever appropriate. In the temporal order memory tests, the temporal order memory index was analyzed using independent Student's *t*-tests (two-tailed), whereas the relative amount of time exploring the objects in sample phases 1 and 2 of the test were analyzed using chi-square (χ^2) tests. In the contextual fear conditioning and extinction test, percent time freezing during the habituation and conditioning phases (day 1) were analyzed using 2 × 6 (treatment × bins) and 2 × 9 (treatment × bins) repeated-measures ANOVAs, respectively, whereas percent time freezing during the expression phase (day 2) was analyzed using 2 × 12 (treatment × bins) repeated-measures ANOVAs. The extinction rate was analyzed using 2 × 4 (treatment × days) repeated-measures ANOVAs, followed by Tukey's post-hoc for multiple comparisons.

Table 3
List of mouse TaqMan gene expression assays used for qRT-PCR analyses.

Gene name	TaqMan assay ID
36B4	Custom-designed
Allograft inflammatory factor 1 (Aif1; = Iba1)	Mm00479862_g1
Chemokine (C-X3-C motif) receptor 1 (Cx3cr1)	Mm00438354_m1
Colony stimulating factor 1 receptor (Csf1r)	Mm01266652_m1
Purinergic receptor P2Y, G-protein coupled 12 (P2ry12)	Mm01950543_s1
Pyrimidinergic receptor P2Y, G-protein coupled, 6 (P2ry6)	Mm02620937_s1
Spi-1 proto-oncogene (Spi1; = Pu.1)	Mm00488140_m1
Triggering receptor expressed on myeloid cells 2 (TREM2)	Mm04209424_g1

The list summarizes the names of the genes of interest and their TaqMan assay ID, listed according to alphabetical order. 36B4 was custom-designed, with the following probe and primer sequences: 36b4 forward primer: 5′-AGATGCAGCAGATCCGCAT-3′; reverse primer: 5′-GTTCTTGC CCATCAGCACC-3′; probe: 5′-CGCTCCGAGGGAAGGCCG-3′.

3. Results

3.1. Validation of local and transient depletion of prefrontal microglia during adolescence in female mice

First, we ascertained the effectiveness, selectivity and transiency of CDS-induced prefrontal microglia depletion during adolescence. To this end, female mice were subjected to a single, bilateral stereotaxic injection of CDS or PBS into the medial portion of the PFC at 6 weeks of age (Fig. 1a). An additional group of female mice receiving sham surgery, which involved the same surgical procedures but no stereotaxic injections at 6 weeks of age, was included as a negative control group as well. The adolescent time period (i.e. 6 weeks of age) was selected based on our previous investigations, demonstrating that transient prefrontal microglia deficiency starting from 6 weeks of age induces an adult emergence of PFC-associated impairments in cognitive functions and synaptic structures in male mice (Schalbetter et al., 2022).

Compared to control mice undergoing sham surgery or control mice receiving a bilateral stereotaxic injection of PBS, CDS-injected mice exhibited a transient reduction in $Iba1^+$ microglial cell numbers in the PFC spanning the infralimbic, prelimbic, and anterior cingulate cortices (Fig. 2a,b). The CDS-induced microglia depletion started to emerge at 1 day post-injection (1 dpi), as supported by the significant main effect of treatment ($F_{(2,12)} = 11.5$, $p < 0.01$) and subsequent post-hoc comparisons between CDS and PBS ($p < 0.01$) or sham ($p < 0.01$) groups. The CDS-induced microglia depletion was most pronounced at 5 dpi (CDS vs. PBS or sham: $p < 0.001$, following ANOVA: $F_{(2,12)} = 139.7$, $p < 0.001$) but was no longer present as of 10 dpi (Fig. 2a). Intra-PFC injection of CDS also led to a transient decrease in microglia density in the primary and secondary motor cortex as well as in the forceps minor of the corpus callosum, but not in the primary somatosensory cortex (Suppl. Fig. S1). Importantly, intra-PFC injection of CDS had no effect on the density of $S100\beta^+$ astrocytes or $NeuN^+$ neurons (Fig. 2c, d). Taken together, these data confirm that a single, bilateral intra-PFC injection of CDS in 6-week-old female mice induces a cell-specific and transient depletion of

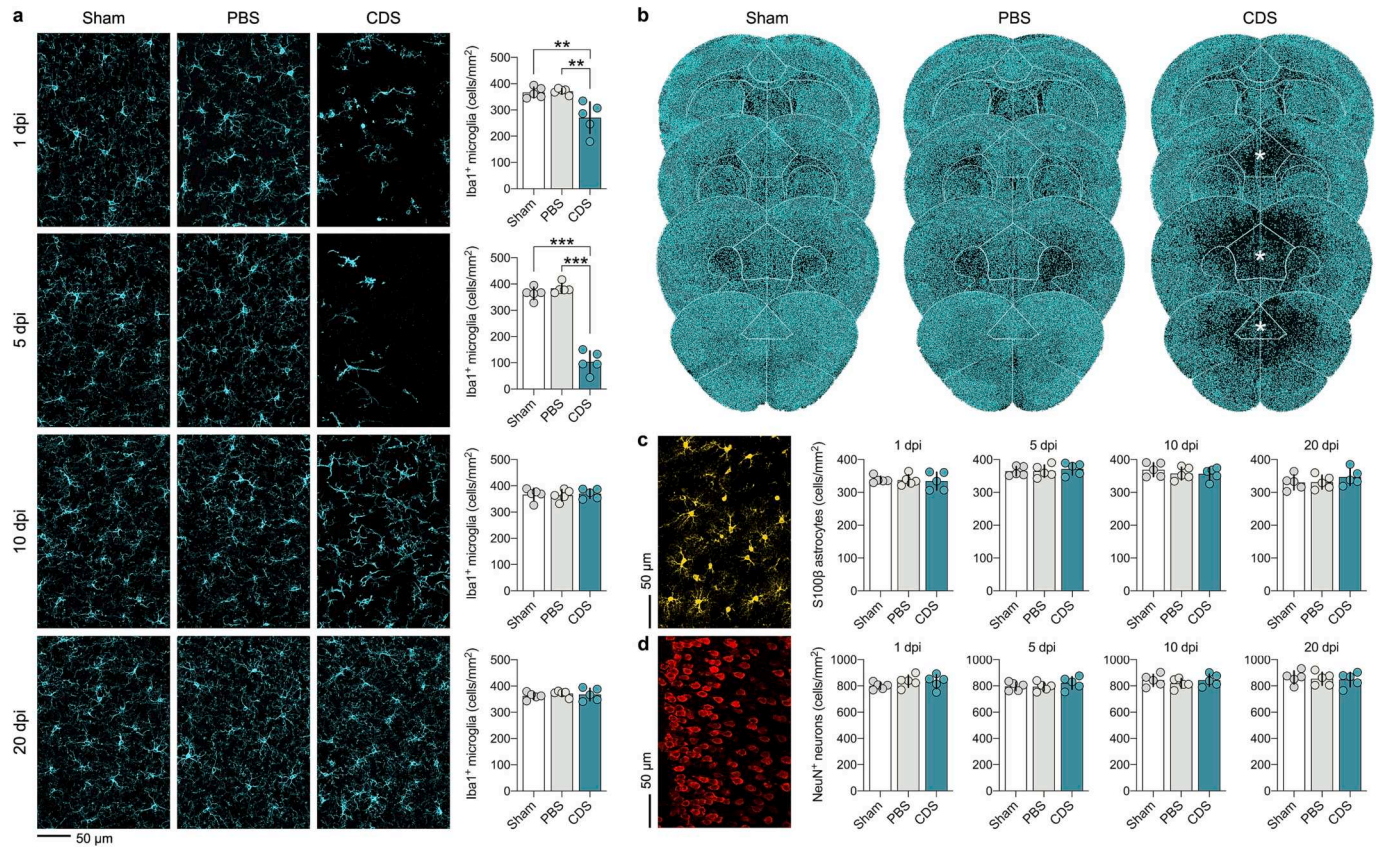

Fig. 2. Validation of local and transient depletion of prefrontal microglia during adolescence in female mice. (a) Representative fluorescent images of Iba1$^+$ microglia in the prefrontal cortex (PFC) of adolescent female mice receiving sham surgery or a bilateral intra-PFC injection of PBS or CDS. The images were taken at 1, 5, 10 and 20 days post-injection (dpi). The bar graphs show the number of Iba1$^+$ microglia in the medial PFC (encompassing infralimbic, prelimbic and anterior cingulate cortices) at the different dpi intervals. $^{**}p < 0.01$ and $^{***}p < 0.001$, based on post-hoc tests following ANOVA; $N = 5$ female mice per group and dpi. (b) Heat scatter representation of the CDS-induced microglia depletion at 5 dpi. The images depict color-coded overlays of coronal PFC sections taken from 5 female mice per group (sham, PBS or CDS), wherein each dot represents an Iba1$^+$ microglial cell. Note the marked reduction of microglial cell density in the medial PFC of CDS-treated female mice, as indicated by the symbol (*) (c) The photomicrograph shows a representative S100β immunofluorescent stain in the PFC region. The bar plots depict the number of S100β$^+$ astrocytes in the medial PFC (encompassing infralimbic, prelimbic and anterior cingulate cortices) of female sham control mice, PBS control mice and CDS mice at different dpi intervals. $N = 5$ female mice per group and dpi. (d) The photomicrograph shows a representative NeuN immunofluorescent stain in the PFC region. The bar plots depict the number of NeuN$^+$ neurons in the medial PFC (encompassing infralimbic, prelimbic and anterior cingulate cortices) of female sham control mice, PBS control mice and CDS mice at different dpi intervals. $N = 5$ female mice per group and dpi. All data are means ± SEM with individual values overlaid.

prefrontal microglia during a restricted window of adolescence.

To further ascertain the transiency of the effects induced by adolescent CDS treatment, we performed detailed analyses of morphological parameters of surface-rendered microglia, which were reconstructed using Imaris image analysis software (Fig. 3a). These morphological analyses were conducted at 10, 20 and 40 dpi, with 10 and 20 dpi corresponding to intervals when microglia densities normalize after CDS-induced depletion in the PFC (Fig. 2a) and 40 dpi corresponding to the interval when behavioral and cognitive testing started (Fig. 1a). Sholl analysis of surface-rendered microglia at 10 dpi revealed that CDS mice displayed a marked reduction in the number of intersections at 5 to 40-µm distance from the soma center (Fig. 3a), as supported by the main effect of treatment ($F_{(1,8)} = 28.3$, $p < 0.001$) and its interaction with distance intervals ($F_{(11,88)} = 28.5$, $p < 0.001$). At 20 dpi, CDS mice still displayed a reduction in the number of intersections at close proximity to the cell soma (10- to 20 µm distance intervals), but they exhibited an increase in the number of remote intersections to the cell soma (30- to 40 µm distance intervals; Fig. 3a) at this post-injection interval, leading to a significant interaction between treatment and distance intervals ($F_{(11,88)} = 14.8$, $p < 0.001$). At 40 dpi, however, CDS and PBS mice no longer differed in terms of the number of intersections analyzed by Sholl analysis (Fig. 3a). Consistent with these dynamic alterations in the complexity of microglial processes, we found that microglia from CDS-treated mice displayed a significant reduction in the total number of branching points ($t_{(8)} = 4.66$, $p < 0.01$) and a significant increase in cell soma area ($t_{(8)} = 3.29$, $p < 0.05$) at 10 dpi, whereas these effects were no longer present at the 20 and 40 dpi intervals (Fig. 3b, c).

To further confirm the transiency of the CDS-induced effects at the level of microglial gene expression, we quantified microglia-defining genes (*Csf1r*, *Cx3cr1*, *Iba1*, *P2ry12*, *P2ry6*, *Pu.1*, and *Trem2*) in MACS-isolated prefrontal microglia. Microglial cells were harvested from the PFC of PBS- and CDS-treated or sham-operated mice at 40 dpi, which corresponds to the interval when behavioral and cognitive testing started (Fig. 1a). These analyses revealed no group differences in the expression of any of the microglia-defining genes, as measured in the adult PFC (Fig. 3d). Hence, a bilateral stereotaxic injection of CDS into the PFC of adolescent female mice does not appear to cause lasting transcriptional changes in microglial cells of the adult PFC.

3.2. *Effects of prefrontal microglia deficiency during adolescence on behavioral and cognitive functions at adult age*

After confirming the effectiveness, selectivity and transiency of CDS-induced prefrontal microglia depletion (Fig. 2,3), we examined whether

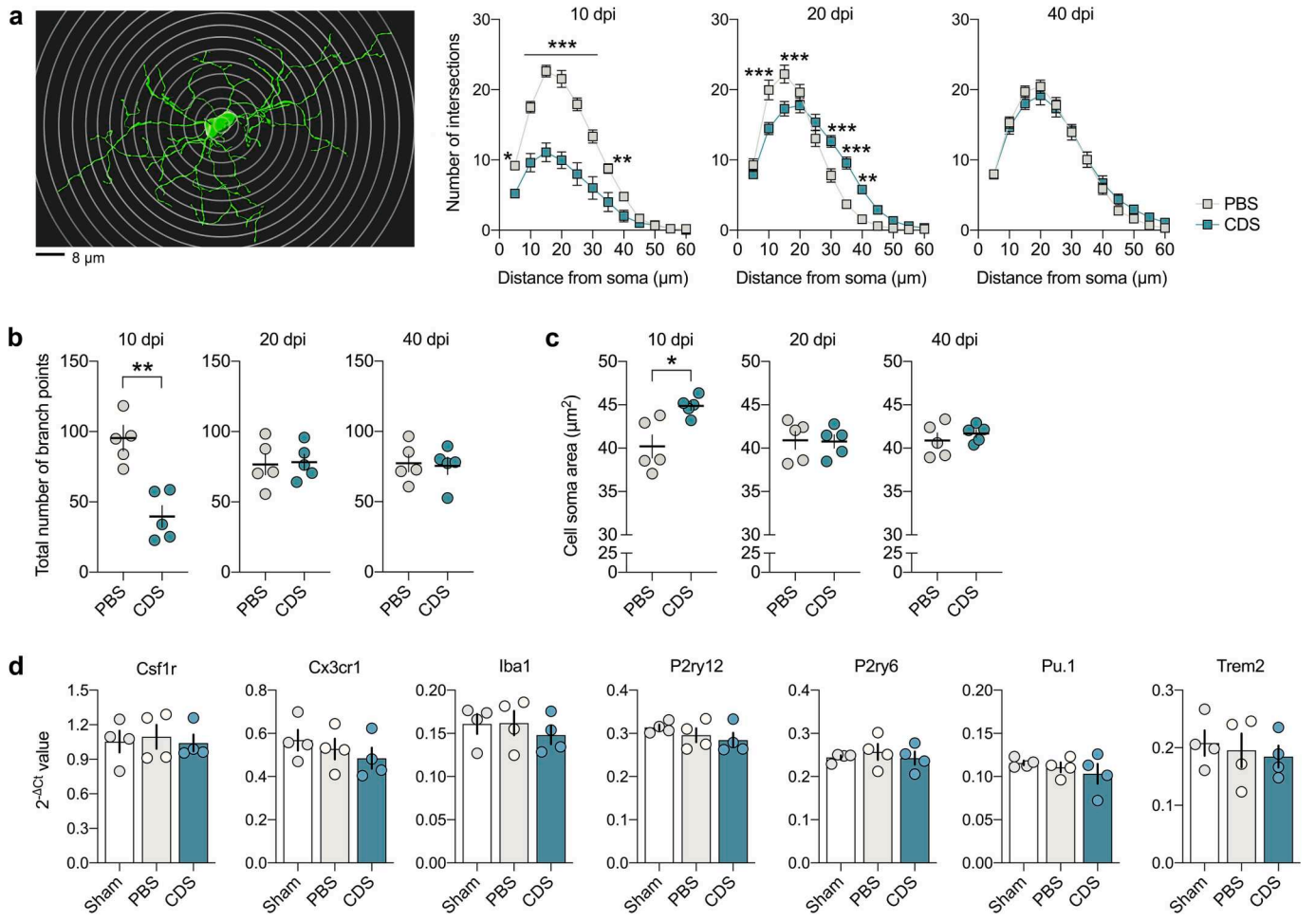

Fig. 3. Morphological parameters and transcriptomic signatures of repopulated microglia after transient depletion of prefrontal microglia during adolescence in female mice. (a) Sholl analysis of surface-rendered microglia, which were reconstructed using Imaris image analysis software, was performed to assess the branching of microglial processes and to estimate the cell soma size of microglia at 10, 20 and 40 days post-injection (dpi) in PBS- and CDS-treated mice. The photomicrograph shows a representative microglial cell after surface rendering and reconstruction with Imaris image analysis software, with digitally applied concentric spheres (5 µm spacing) from the soma center for subsequent Sholl analysis. The line plots depict the number of microglial processes intersecting at sequential radial distances from soma at each dpi interval of interest. *$p < 0.05$, **$p < 0.01$ and ***$p < 0.001$, based on Bonferroni post-hoc tests following significant 2-way interactions in ANOVA; $N = 5$ female mice per group and dpi. (b) Total number of branch points of prefrontal microglia in PBS- and CDS-treated mice at the 10, 20 and 40 dpi intervals. **$p < 0.01$, based on independent *t*-tests (two-tailed); $N = 5$ female mice per group and dpi. (c) Average cell soma area of prefrontal microglia in PBS- and CDS-treated mice at the 10, 20 and 40 dpi intervals. *$p < 0.05$, based on independent *t*-tests (two-tailed); $N = 5$ female mice per group and dpi. (d) Microglia-defining genes were analyzed in prefrontal microglia isolated from PBS- and CDS-treated or sham-operated mice at 40 dpi, which corresponds to the interval when behavioral and cognitive testing started. The bar plots show mRNA levels of Csf1r, Cx3cr1, Iba1 (=Aif1), P2ry12, P2ry6, Pu.1 (=Spi1) and Trem2. Each data point corresponds to pooled samples from 3 female mice, with 4 independent replicates per group. All data are means ± SEM with individual values overlaid.

behavioral and cognitive development in female mice is influenced by prefrontal microglia deficiency during adolescence. To this aim, 6-week-old female mice were subjected to intra-PFC CDS or PBS injections, after which they were allowed to mature until adulthood. Behavioral testing commenced at 12 weeks of age (Fig. 1a).

There were no group differences in terms of locomotor activity scores or indices of innate anxiety-like behavior in the open field (Fig. 4a, Suppl. Table 1) and light–dark box (Fig. 4b) tests, indicating that the adolescent CDS treatment did not lead to alterations in these behavioral domains at adult age. In phase 1 of the social interaction test, in which the animals were allowed to freely explore a non-familiar mouse or inanimate dummy object, PBS and CDS groups similarly displayed a clear preference toward the non-familiar mouse (Fig. 4c). Repeated-measures ANOVA of the absolute time exploring the non-familiar mouse or dummy object only revealed a significant main effect of object ($F_{(1,18)} = 73.2, p < 0.001$). Likewise, there were no group differences in phase 2 of the social interaction test, in which the animals were allowed to explore a novel versus familiarized mouse (Fig. 4c). PBS and CDS groups similarly displayed a clear preference toward the novel mouse in phase 2 of the test (Fig. 4c), as supported by the significant main effect of novelty ($F_{(1,18)} = 21.8, p < 0.001$) in repeated-measures ANOVA of the absolute time exploring the novel mouse or familiarized mouse. Hence, adolescent CDS treatment in female mice did not alter social approach behavior or social recognition memory in adulthood.

As shown in Fig. 4d, however, adult female mice subjected to adolescent CDS treatment displayed an impairment in their capacity to discriminate the relative recency of objects, as assessed using the temporal order memory test for objects. In this test, PBS and CDS mice were first allowed to freely explore a first pair of identical objects (sample phase 1) and then a novel pair of identical objects (sample phase 2). In the subsequent test phase, when the mice were allowed to choose between one object from the first pair (temporally remote objects) and one from the second pair (temporally recent objects), only PBS mice showed a preference toward the temporally remote object, whereas CDS mice failed to discriminate between the two objects (Fig. 4d; temporal order

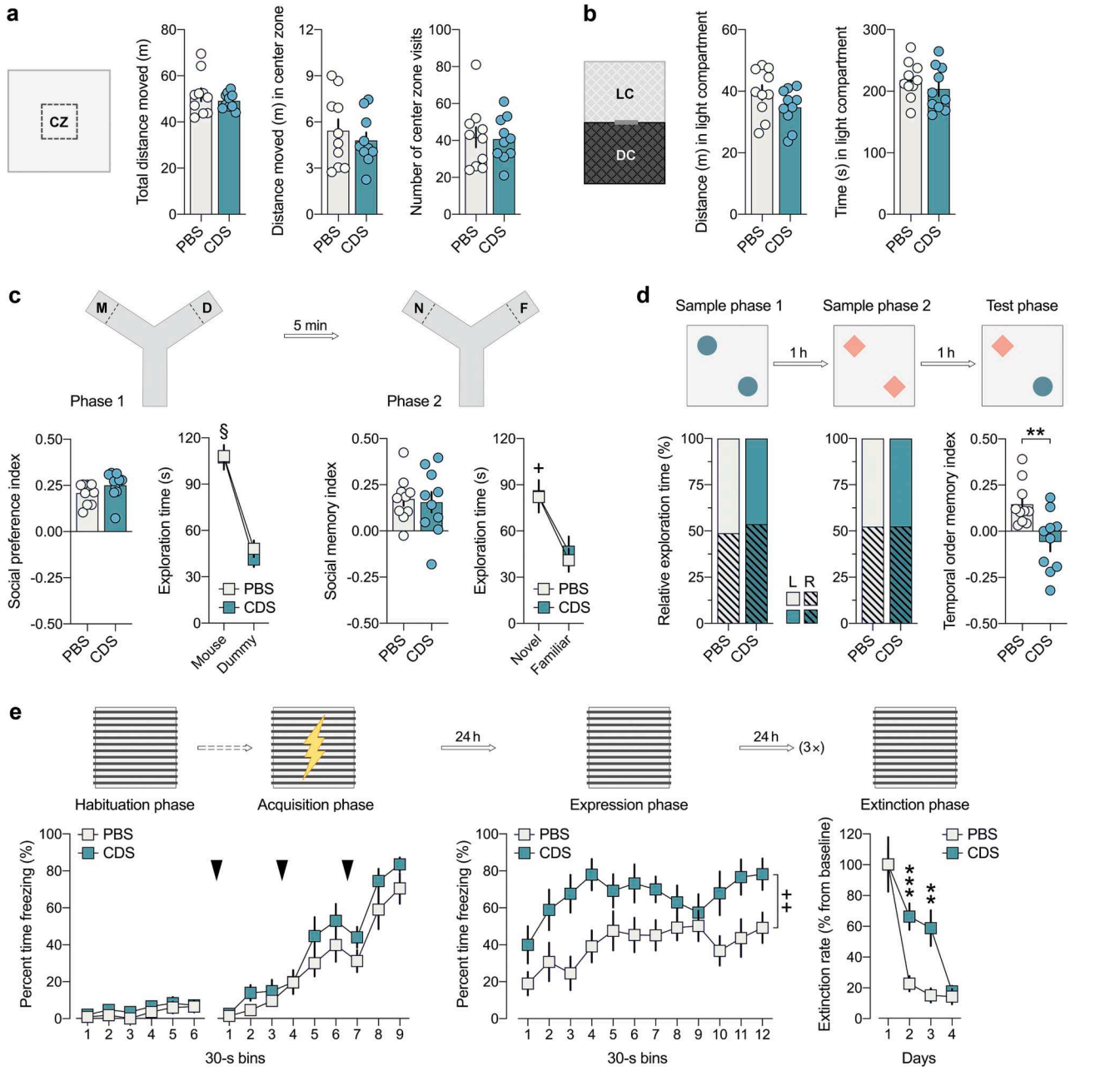

Fig. 4. Effects of prefrontal microglia deficiency during adolescence on adult behavioral and cognitive functions in female mice. To examine possible effects of prefrontal microglia depletion during adolescence on adult behavioral and cognitive functions, 6-week-old female mice were injected with either CDS or PBS and were allowed to recover for 6 weeks. Behavioral and cognitive testing commenced when the animals reached 12 weeks of age. (a) Total distance moved, distance moved in the center zone (CZ) and number of CZ visits in PBS and CDS mice during the open field test. (b) Distance moved and time spent in the light compartment (LC) in female PBS and CDS mice during the light–dark box test, which measures the animals' exploration of the LC relative to the dark compartment (DC). (c) Phase 1 (D = dummy object, M = unfamiliar mouse) and phase 2 (F = familiar mouse; N = novel mouse) of the social interaction test. The bar plots show the social preference index in phase 1 (values > 0 represent a preference toward the unfamiliar mouse) and social memory index in phase 2 (values > 0 represent a preference toward the novel mouse), whereas the line plots depict absolute exploration times in either phase. $^{\S}p < 0.001$, reflecting the overall main effect of object in phase 1; $^{+}p < 0.001$, reflecting the overall main effect of novelty in phase 2, based on repeated-measures ANOVA. (d) The percentage bar plots represent the relative amount of time (%) exploring the left (L) or right (R) object in sample phase 1 and 2 of the temporal order memory test. The bar plot shows the temporal order memory index during the test phase (values > 0 represent a preference toward the temporally more remote object presented in sample phase 1). $^{**}p < 0.01$, based on independent *t*-test (two-tailed). (e) Acquisition, expression and extinction of contextual fear. The line plots show percent time freezing during habituation, acquisition and expression, as well as the extinction rate (% change from freezing levels measured during the expression phase). The arrows indicate the presentation of a mild electric foot shock. $^{++}p < 0.01$, reflecting the main effect of treatment in repeated-measures ANOVA. $^{**}p < 0.01$ and $^{***}p < 0.001$, based on post-hoc tests following repeated-measures ANOVA. All data are means ± SEM with individual values overlaid; $N = 10$ female mice in each group and test.

memory index in PBS vs. CDS mice: $t_{(18)} = 3.08$, $p < 0.01$). Additional analyses of the relative amount of time exploring the objects in sample phases 1 and 2 of the temporal order memory test revealed no effects of CDS on object exploration per se (Fig. 4d), suggesting that the CDS-induced disruption of temporal order memory represents a genuine deficit in the capacity of CDS mice to discriminate the relative recency of stimuli.

In the contextual fear conditioning test, the initial acquisition of

conditioned fear, which was measured by the percentage time freezing across successive presentations of mild electric foot shocks on day 1 of the test, was similar between PBS and CDS mice (Fig. 4e). Compared to PBS controls, however, CDS-treated mice displayed an overall increase with regard to the expression of conditioned fear toward the context, which was assessed 24 h after conditioning (Fig. 4e). Repeated-measures ANOVA of percent time freezing during the expression phase revealed significant main effects of bins ($F_{(11,198)} = 3.32$, $p < 0.001$) and treatment ($F_{(1,18)} = 8.29$, $p < 0.01$). In addition, CDS-treated mice displayed a deficit in the extinction of contextual fear memory, which was assessed by comparing the relative amount of conditioned freezing during successive days of context exposures relative to baseline freezing measured 24 h after conditioning (Fig. 4e). Repeated-measures ANOVA of the relative amount of conditioned freezing during extinction training revealed a significant main effect of days ($F_{(3,54)} = 38.91$, $p < 0.001$) and a significant interaction between treatment and days ($F_{(3,54)} = 4.45$, $p < 0.01$). Subsequent post-hoc comparisons confirmed a significant difference between PBS and CDS mice at days 2 ($p < 0.001$) and 3 ($p < 0.01$) of extinction training (Fig. 4e).

To examine whether the stereotaxic surgery per se may have confounded the identified effects of CDS-induced prefrontal microglia depletion on cognitive development (Fig. 4), we compared the behavioral performance of adult female mice that received no stereotaxic injection (sham control mice) and female mice that were subjected to a bilateral stereotaxic injection of PBS at 6 weeks of age. These additional analyses revealed no differences between sham-treated and PBS-injected mice in terms of basal locomotor activity or indices of innate anxiety-like behavior, as analyzed by open-field (Suppl. Fig. S2a) and light–dark box (Suppl. Fig. S2b) tests. Likewise, sham-treated and PBS-injected mice did not differ in the tests assessing social approach behavior and social recognition memory (Suppl. Fig. S2c), temporal order memory (Suppl. Fig. S2d), or contextual fear conditioning and extinction (Suppl. Fig. S2e). These data show that the selected stereotaxic method did not induce any noticeable effects on behavioral and cognitive development, suggesting that the CDS-induced impairments in temporal order memory and contextual fear expression and extinction represent genuine long-term effects of prefrontal microglia depletion during adolescence.

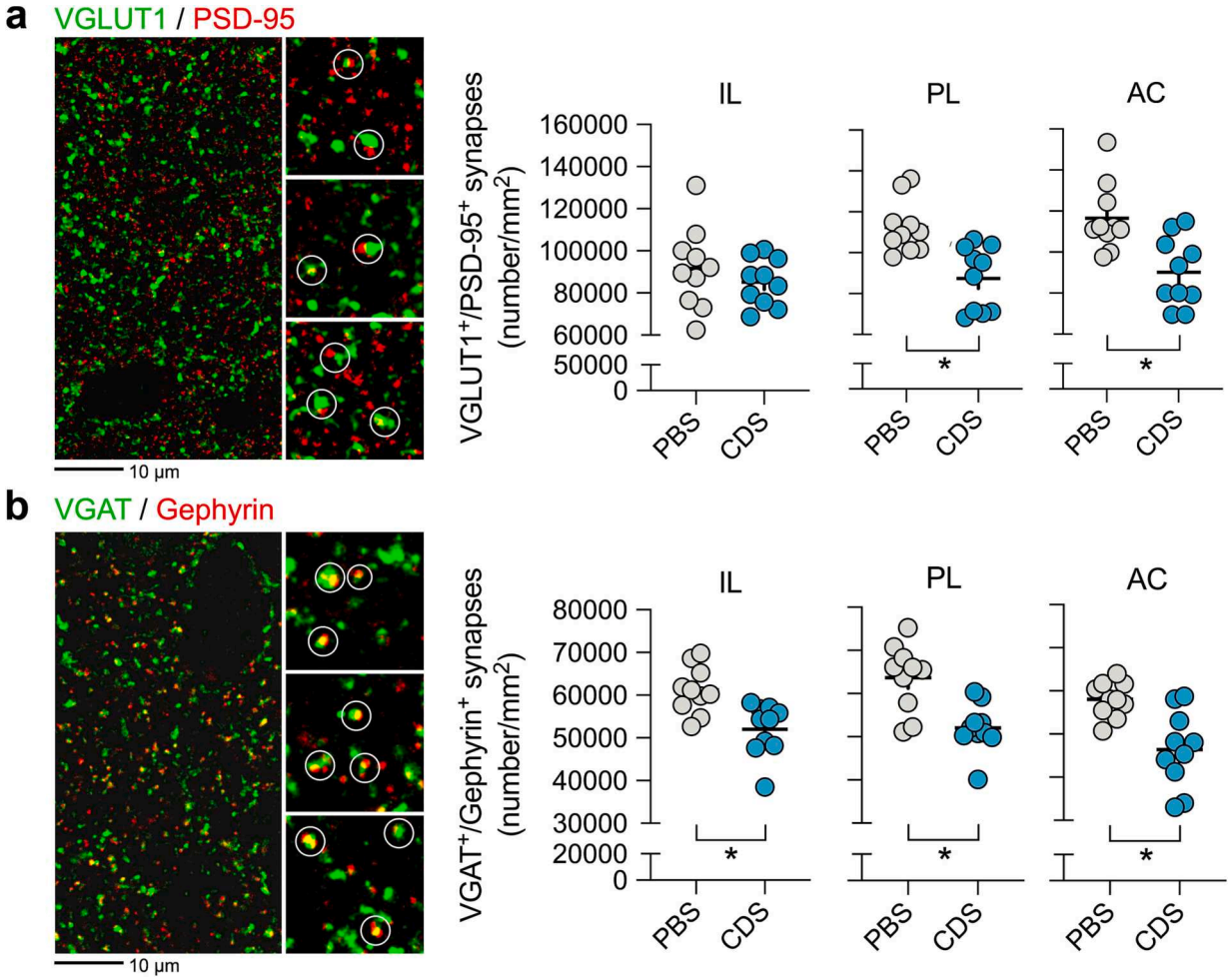

Fig. 5. Effects of prefrontal microglia deficiency during adolescence on synaptic densities in the adult prefrontal cortex. To examine possible effects of prefrontal microglia depletion during adolescence on synaptic densities in the adult prefrontal cortex, 6-week-old female mice were injected with either CDS or PBS and were allowed to recover for 6 weeks. Synaptic densities were quantified when the animals reached 12 weeks of age. (a) The photomicrograph shows a representative double-immunofluorescence stain using VGLUT1 (green) as presynaptic and PSD-95 (red) as postsynaptic markers of excitatory neurons. Examples of VGLUT1$^+$/PSD-95$^+$ co-localizing synapses are highlighted by white circles in magnified sections. The scatter plots show the density (number/mm^2) of VGLUT1$^+$/PSD-95$^+$ excitatory synapses in infralimbic (IL), prelimbic (PL) and anterior cingulate (AC) subregions of the prefrontal cortex from PBS and CDS mice. *$p < 0.05$, based on independent *t*-tests (two-tailed). (b) The photomicrograph shows a representative double-immunofluorescence stain using VGAT (green) as presynaptic and Gephyrin (red) as postsynaptic markers of inhibitory neurons. Examples of VGAT$^+$/Gephyrin$^+$ co-localizing synapses are highlighted by white circles in magnified sections. The scatter plots display the density (number/mm^2) of VGAT$^+$/Gephyrin$^+$ inhibitory synapses in IL, PL and AC subregions of the prefrontal cortex from PBS and CDS mice. *$p < 0.05$, based on independent *t*-tests (two-tailed). $N = 10$ female mice per group.

3.3. Effects of prefrontal microglia deficiency during adolescence on synaptic densities in the adult PFC

Based on our previous findings in male mice (Schalbetter et al., 2022), we next investigated whether transient microglia depletion during adolescence is sufficient to cause lasting synaptic changes in female mice. Using colocalization analyses of presynaptic and postsynaptic markers, we estimated the density of excitatory and inhibitory synapses in the PFC of adult (12-week-old) female mice that were subjected to PBS or CDS treatment at 6 weeks of age. For excitatory synapses, we used the presynaptic marker vesicular glutamate transporter 1 (VGLUT1) and the postsynaptic marker postsynaptic density protein 95 (PSD-95) (Berry and Nedivi, 2017), whereas vesicular γ-aminobutyric acid transporter (VGAT) and Gephyrin (Choii and Ko, 2015) were used as inhibitory presynaptic and postsynaptic markers, respectively.

As shown in Fig. 5a, adolescent CDS treatment decreased the density of VGLUT1$^+$/PSD-95$^+$ excitatory synapses in the prelimbic ($t_{(18)} = 2.18$, $p < 0.05$) and anterior cingulate ($t_{(18)} = 2.68$, $p < 0.05$) subregions of the PFC, whereas it did not alter VGLUT1$^+$/PSD-95$^+$ synaptic density in the infralimbic subregion. Moreover, adolescent CDS treatment reduced the density of VGAT$^+$/Gephyrin$^+$ inhibitory synapses in the infralimbic ($t_{(18)} = 2.24$, $p < 0.05$), prelimbic ($t_{(18)} = 2.35$, $p < 0.05$) and anterior cingulate ($t_{(18)} = 2.28$, $p < 0.05$) subregions of the PFC (Fig. 5b). Thus, these data demonstrate that transient prefrontal microglia depletion during adolescence exerts lasting effects on the density of both excitatory and inhibitory synapses in the PFC of adult female mice.

3.4. Windows of vulnerability for cognitive and synaptic sequelae after prefrontal microglia deficiency

To further explore whether adolescence is a window of increased vulnerability for cognitive and synaptic sequelae after transient microglia deficiency (Schalbetter et al., 2022), we applied the same microglia-depleting manipulation to adult female mice (12 weeks of age) and examined possible effects on behavior and cognition (Fig. 1b) Consistent with the effects induced by the adolescent CDS treatment (Fig. 2), intra-PFC injection of CDS in adult mice caused a 70 to 80% decrease ($t_{(8)} = 17.71$, $p < 0.001$) in the prefrontal density of Iba1$^+$ microglial cells at the 5 dpi interval (Fig. 6a). Similar to when CDS was applied to adolescent mice (Fig. 2), the CDS-induced microglia depletion in adulthood was transient and was no longer apparent at 20 dpi in terms of prefrontal microglial cell density (Fig. 6a). Consistent with the selective effects induced by the adolescent CDS treatment (Fig. 2), intra-PFC injection of CDS in adult mice did not alter the prefrontal density of S100β$^+$ astrocytes (Fig. 6b) or NeuN$^+$ neurons (Fig. 6c).

Despite the efficacy of the adult CDS treatment to transiently deplete microglia from the adult PFC, this manipulation did not alter behavioral or cognitive functions after microglia repopulation. Indeed, there were no differences between female mice subjected to adult PBS or CDS treatment in terms of basal locomotor activity or indices of innate anxiety-like behavior, as analyzed by open-field (Fig. 7a) and light–dark box (Fig. 7b) tests. Likewise, female mice receiving an intra-PFC injection of PBS or CDS in adulthood did not differ in the tests assessing social approach behavior and social recognition memory (Fig. 7c), temporal order memory (Fig. 7d), or contextual fear conditioning and extinction (Fig. 7e).

Consistent with the lack of behavioral and cognitive effects, intra-PFC administration of CDS in adulthood did not alter the prefrontal density of VGLUT1$^+$/PSD-95$^+$ excitatory synapses (Fig. 8a) or VGAT$^+$/Gephyrin$^+$ inhibitory synapses in female mice (Fig. 8b). Taken together, these data demonstrate that the adult female PFC, unlike the adolescent PFC, is resilient to transient microglia deficiency in terms of lasting behavioral, cognitive and synaptic maladaptations.

4. Discussion

Adolescent maturation of the PFC is necessary for acquiring mature cognitive abilities in adulthood (Caballero et al., 2016; Larsen and Luna, 2018; Nabel et al., 2020; Falk et al., 2021). Using a model of cell-specific, transient and local depletion of microglia during restricted time windows of adolescence, our previous study showed that microglia actively contribute to this maturational process in male mice (Schalbetter et al., 2022). Here, we used the same model to demonstrate that a temporary deficiency of prefrontal microglia during adolescence is sufficient to cause an adult emergence of synaptic and cognitive impairments in female mice. We further show that inducing local and transient microglia depletion in the adult PFC of female mice does not lead to lasting behavioral, cognitive and synaptic maladaptations. The timing-dependent effects revealed here and before (Schalbetter et al., 2022) are unlikely to be the result of a varying degree of microglia depletion, as intra-PFC injections of CDS in adolescence or adulthood caused a highly comparable degree of microglia depletion (70 to 80% reduction at the peak of the depletion at both ages). Rather, the differential impact of adolescent or adult CDS treatment on cognition and synaptic structures may be accounted for by a timing-dependent disruption of ongoing maturational processes. Taken together, our previous (Schalbetter et al., 2022) and present investigations identify adolescence as a critical period during which prefrontal microglia act on cognitive development and synaptic refinement in both males and females.

Prefrontal microglia deficiency during adolescence was found to cause adult impairments in temporal order memory in both males (Schalbetter et al. 2022) and females (Fig. 4d). Temporal behavioral

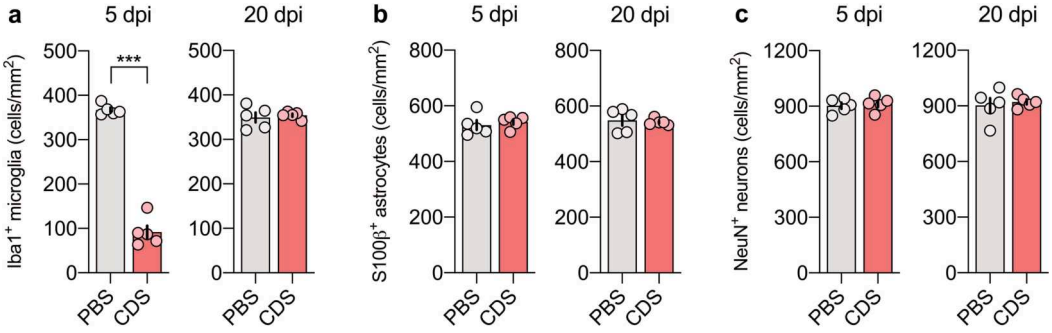

Fig. 6. Density of microglia, neurons and astrocytes during prefrontal microglia depletion in adulthood. Post-mortem immunohistochemistry was used to assess whether bilateral stereotaxic injection of CDS into the prefrontal cortex of adult (12-week-old) female mice alters the density of microglia, neurons and astrocytes in the medial portion of the prefrontal cortex (encompassing infralimbic, prelimbic and anterior cingulate subregions) at 5 and 20 days post-injection (dpi). (a) Number of Iba1$^+$ microglia in the PBS and CDS groups at 5 and 20 dpi. ***$p < 0.001$, based on independent *t*-test (two-tailed). (b) Number of S100β$^+$ astrocytes in the PBS and CDS groups at 5 and 20 dpi. (c) Number of NeuN$^+$ neurons in the PBS and CDS groups at 5 and 20 dpi. All data are means ± SEM with individual values overlaid; $N =$ 5 female mice per group and dpi.

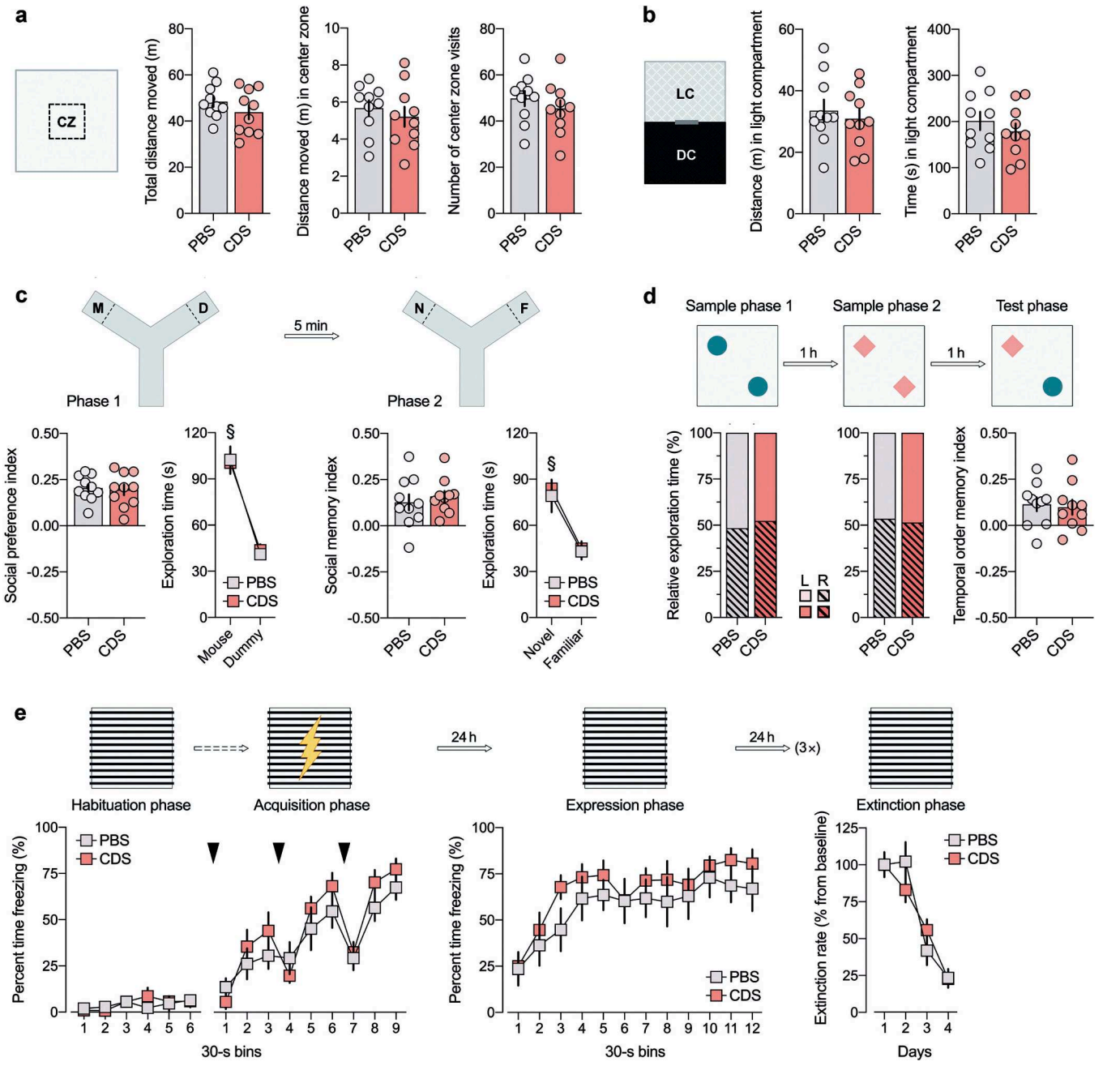

Fig. 7. No effects of transient microglia depletion in the adult prefrontal cortex on behavioral and cognitive functions. To examine possible effects of prefrontal microglia depletion in adulthood on behavioral and cognitive functions, 12-weeks-old female mice were injected with either CDS or PBS and were allowed to recover for 6 weeks. Behavioral and cognitive testing commenced when the animals reached 18 weeks of age. (a) Total distance moved, distance moved in the center zone (CZ) and number of CZ visits in PBS and CDS mice during the open field test. (b) Distance moved and time spent in the light compartment (LC) in female PBS and CDS mice during the light–dark box test, which measures the animals' exploration of the LC relative to the dark compartment (DC). (c) Phase 1 (D = dummy object, M = unfamiliar mouse) and phase 2 (F = familiar mouse; N = novel mouse) of the social interaction test. The bar plots show the social preference index in phase 1 (values > 0 represent a preference toward the unfamiliar mouse) and social memory index in phase 2 (values > 0 represent a preference toward the novel mouse), whereas the line plots depict absolute exploration times in either phase. $^{\S}p < 0.001$, reflecting the overall main effect of object in phase 1 or 2 of the test. (d) The percentage bar plots represent the relative amount of time (%) exploring the left (L) or right (R) object in sample phase 1 and 2 of the temporal order memory test. The bar plot shows the temporal order memory index during the test phase (values > 0 represent a preference toward the temporally more remote object presented in sample phase 1). (e) Acquisition, expression and extinction of contextual fear. The line plots show percent time freezing during habituation, acquisition and expression, as well as the extinction rate (% change from freezing levels measured during the expression phase). The arrows indicate the presentation of a mild electric foot shock. All data are means ± SEM with individual values overlaid; $N = 10$ female mice in each group and test.

sequencing and temporal ordering of events critically underly the formation and/or expression of this type of memory and are highly sensitive to prefrontal maladaptations, especially within dorsal subregions of the PFC (Delatour and Gisquet-Verrier, 2001; Hannesson et al., 2004; Barker et al., 2007). Male and female mice subjected to prefrontal microglia deficiency during adolescence also developed similar deficits in contextual fear extinction at adult age. It is well known that the PFC strongly regulates the extinction of conditioned fear (Sotres-Bayon et al., 2006), as supported by numerous rodent studies demonstrating impaired fear extinction following inactivation of the PFC (Morgan and

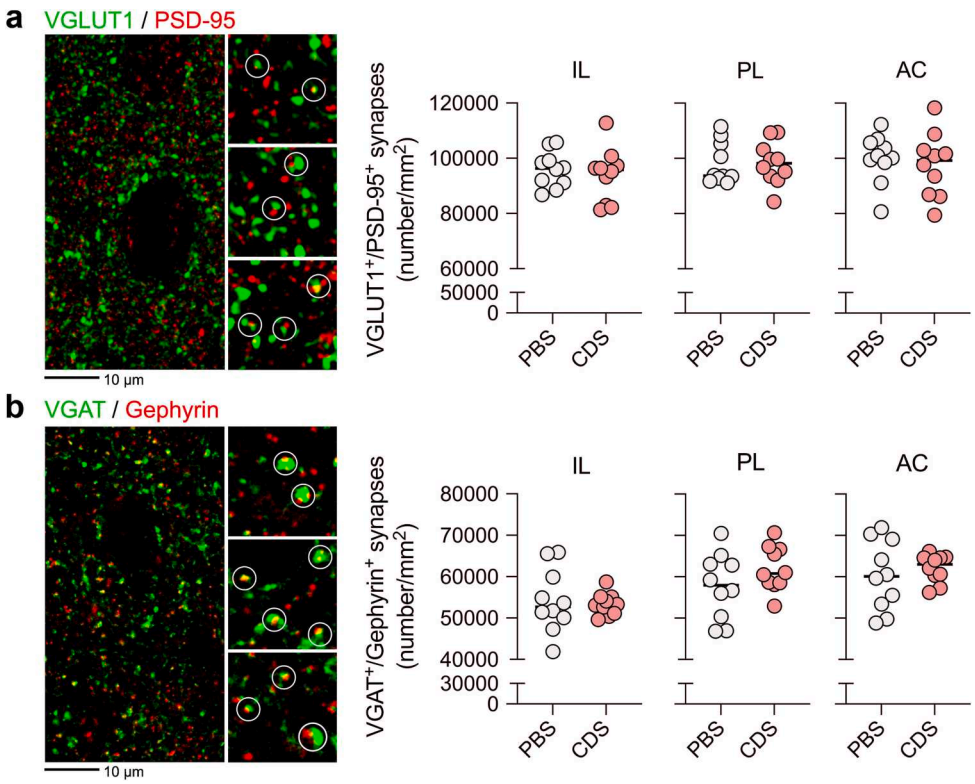

Fig. 8. No effects of prefrontal microglia depletion in adulthood on synaptic densities in the adult prefrontal cortex. To examine possible effects of prefrontal microglia depletion in adulthood on synaptic densities in the adult prefrontal cortex, 12-week-old female mice were injected with either CDS or PBS and were allowed to recover for 6 weeks. Synaptic densities were quantified when the animals reached 18 weeks of age. (a) The photomicrograph shows a representative double-immunofluorescence stain using VGLUT1 (green) as presynaptic and PSD-95 (red) as postsynaptic markers of excitatory neurons. Examples of VGLUT1$^+$/PSD-95$^+$ co-localizing synapses are highlighted by white circles in magnified sections. The scatter plots show the density (number/mm^2) of VGLUT1$^+$/PSD-95$^+$ excitatory synapses in infralimbic (IL), prelimbic (PL) and anterior cingulate (AC) subregions of the prefrontal cortex from PBS and CDS mice. (b) The photomicrograph shows a representative double-immunofluorescence stain using VGAT (green) as presynaptic and Gephyrin (red) as postsynaptic markers of inhibitory neurons. Examples of VGAT$^+$/Gephyrin$^+$ co-localizing synapses are highlighted by white circles in magnified sections. The scatter plots display the density (number/mm^2) of VGAT$^+$/Gephyrin$^+$ inhibitory synapses in IL, PL and AC subregions of the prefrontal cortex from PBS and CDS mice. $N = 10$ female mice per group.

LeDoux, 1995, 1999; Lebrón et al., 2004; Sierra-Mercado et al., 2011). The sex-independent effects of adolescent CDS exposure on temporal order memory and contextual fear extinction suggest that prefrontal microglia deficiency during adolescence similarly disrupts the maturation of the underlying neural substrates in males and females. In support of this notion, intra-PFC administration of CDS during adolescence decreased prefrontal densities of excitatory and inhibitory synapses at adult age, with highly comparable effects emerging in male (Schalbetter et al., 2022) and female (Fig. 5) mice.

Despite these similarities, however, some of the effects induced by prefrontal microglia deficiency during adolescence appear to be sexually dimorphic. Unlike in males (Schalbetter et al., 2022), adolescent CDS treatment had no effect on adult social recognition memory in female mice (Fig. 4c). Furthermore, female mice subjected to prefrontal microglia depletion during adolescence not only displayed impaired extinction of contextual fear memory, but also they exhibited an overall increase in the expression of conditioned fear toward the context, in which aversive conditioning took place (Fig. 4e). In male mice, adolescent CDS treatment did not alter the expression of conditioned fear toward the context, but only led to a selective deficit in subsequent fear extinction (Schalbetter et al., 2022). Whereas the PFC critically regulates the extinction of conditioned fear (Morgan and LeDoux, 1995, 1999; Lebrón et al., 2004; Sotres-Bayon et al., 2006; Sierra-Mercado et al., 2011), the initial expression of contextual fear responses is governed by the activity of hippocampal-amygdalar circuits (Maren et al., 2013). On speculative grounds, the concomitant effects of adolescent CDS treatment on contextual fear expression and extinction in female mice may indicate that the transient microglia depletion during adolescence may not only have disrupted the maturation of the PFC itself, but also it may have induced additional mal-adaptive effects on interconnected structures, such as the hippocampus and amygdala. On the other hand, the more selective effect of adolescent CDS treatment on contextual fear extinction in male mice suggests that prefrontal microglia deficiency during male adolescence has a more restricted impact on the maturation of prefrontal circuitries while largely sparing interconnected structures. Additional studies exploring neuronal deficits in multiple cortical and subcortical brain areas are required to test this hypothesis further.

There are various plausible mechanisms by which transient microglia depletion during adolescence could induce lasting effects on adult brain functions. Consistent with the emerging role of microglia in synaptic refinement (Schafer et al., 2012; Hong et al., 2016; Cheadle et al., 2020), the findings from our previous study in male mice suggest that prefrontal microglia deficiency may influence cognitive development by means of refining dendritic and synaptic structures (Schalbetter et al., 2022). In support of this notion, we identified dynamic changes in microglia-mediated synaptic engulfment after transient microglia deficiency in the adolescent PFC (Schalbetter et al., 2022). Interestingly, while there was an initial decrease in the uptake of synaptic particles into prefrontal microglia shortly after the peak of their depletion (i.e., at 10 dpi), this decrease was followed by a phase of increased synaptic engulfment by prefrontal microglia (Schalbetter et al., 2022). The latter may provide a parsimonious explanation for the seemingly paradoxical effects of transient microglia deficiency on decreasing, rather than increasing, synaptic densities in the adult PFC of both male (Schalbetter et al., 2022) and female (Fig. 5) mice. Besides microglia-mediated synaptic pruning, however, several alternative (but not mutually exclusive) mechanisms may contribute to the emergence of adult cognitive and synaptic deficits following prefrontal microglia depletion during adolescence. These may involve reactive astrocytes, which may be instructed by (transient) microglial Trem2 deficiency to over-prune synapses (Jay et al., 2019; Konishi et al., 2020), and/or by a transient deficiency in microglia-derived neurotrophic factors, which appear to promote synaptic remodeling (Parkhurst et al., 2013). In addition, transient microglia depletion during adolescence may reduce adult synaptic densities through its effects on extracellular matrix (ECM) components. Indeed, our previous study in male mice demonstrated that CDS-induced microglia depletion during adolescence led to an

upregulation of ECM genes, many of which persisted into adulthood. Consistent with these effects, a recent study in mice showed that microglia actively engulf ECM proteins, such that a loss of microglia is associated with impaired ECM engulfment and a concomitant accumulation of ECM proteins in close contact with synapses (Nguyen et al., 2020). The latter has further been associated with impaired synaptic plasticity and cognitive functions (Nguyen et al., 2020).

Previous findings suggest that repopulated microglia may not necessarily be identical to the original microglial population (Huang et al., 2018). Therefore, it is possible that the effects of adolescent CDS treatment on brain and behavior may be, at least in part, accounted for by a different microglial phenotype after repopulation, rather than by the transient prefrontal microglia depletion per se. While our study cannot rule out this possibility completely, we did not find evidence for different microglial phenotypes persisting into adult life after adolescent depletion and subsequent repopulation. We quantified key genes pertaining to microglial homeostasis and reactivity (*Csf1r*, *Cx3cr1*, *Iba1*, *P2ry12*, *P2ry6*, *Pu.1*, and *Trem2*) in prefrontal microglia isolated from adult female mice that were subjected to CDS, PBS or sham treatment in adolescence. These analyses revealed no group differences in the expression of any of these genes. Hence, consistent with its transient effects on microglial cell density, a bilateral stereotaxic injection of CDS into the PFC of adolescent female mice did not appear to cause lasting transcriptional changes in key genes relevant for microglial homeostasis and reactivity. Moreover, our morphological analyses of repopulated microglia demonstrated that there were no morphological changes at the 40 dpi interval, which corresponded to the dpi interval when behavioral and cognitive assessment started. There were, however, transient morphological changes of microglia at earlier dpi intervals (10 and 20 dpi). Our findings suggest that microglia densities normalize as early as 10 dpi after CDS treatment, but repopulated microglial cells appear to take longer in reattaining the morphological characteristics of microglia from PBS-treated control animals. Importantly, our findings also demonstrate that CDS-induced prefrontal microglia depletion in adult female mice fails to induce significant effects on synaptic densities and cognitive functions, whereas marked effects emerged when the same manipulation was implemented in adolescence. These timing-dependent effects are consistent with our previous findings in male mice (Schalbetter et al., 2022) and are unlikely to be the result of a varying degree of the depletion, as intra-PFC injections of CDS in adolescence or adulthood caused a highly comparable amount of microglia depletion (70 to 80% reduction at the peak of the depletion under both conditions). Taken together, our previous (Schalbetter et al., 2022) and present findings provide converging evidence suggesting that transient prefrontal microglia depletion in adolescence interfers with maturational processes occurring between adolescence and adulthood. It is conceivable that transient deficiency of microglia during critical stages of prefrontal maturation sets in motion a number of secondary or down-stream effects in various cell populations (including neurons and astrocytes), which together disrupt normal synaptic and cognitive maturation. Future investigations will be needed to identify these secondary or down-stream effects.

Several genetic and pharmacological models of microglia depletion exist (Ginhoux et al., 2010; Kierdorf et al., 2013; Parkhurst et al., 2013; Elmore et al., 2014; Torres et al., 2016; Masuda et al., 2020). The model presented here and before (Schalbetter et al., 2022) is, however, unique in that it allows for a selective manipulation of microglia in a brain region-specific and temporally restricted manner without inducing nonspecific effects on peripheral immune cells. This degree of specificity is not reached by other models, be it because they lack brain region specificity and/or are associated with a suppression or depletion of peripheral immune cells, including monocytes and macrophages (Ginhoux et al., 2010; Kierdorf et al., 2013; Parkhurst et al., 2013; Elmore et al., 2014; Masuda et al., 2020). Of note, many other previous studies used clodronate liposome preparations (Kumamaru et al., 2012; Han et al., 2019; Jacobs et al., 2019), whereas the present study and our previous research (Schalbetter et al., 2022) used the clodronate salt preparation (i.e. CDS) without liposomal encapsulation. The reason why we selected CDS, rather than the liposomal preparation, was because of previous findings indicating that liposomes may cross the cell membrane of non-phagocytotic or less phagocytotic cells such as neurons, blood vessels and astrocytes, thereby inducing off-target effects on other cells (Han et al., 2019). Unlike liposomal preparations, the chemical properties of the salt preparation of clodronate (i.e. CDS) readily prevent its passive diffusion across cell membranes, so that CDS is taken up primarily by cells with strong innate phagocytic activity, such as microglia. Thus, intracerebral injection of CDS reaches more cellular specificity than clodronate liposome preparations. This notion is supported by our previous transcriptomic analyses conducted in male mice (Schalbetter et al., 2022), which revealed a selective reduction in microglia-defining genes after intracerebral injection of CDS, whereas genes defining other major cell populations, including astrocytes, oligodendrocytes, endothelial cells, and neurons, were not significantly affected by the CDS treatment. Our immunohistochemical analyses of microglial and non-microglial cells confirmed these selective effects, suggesting that intracerebral injection of CDS, as used in the present study, is indeed selective to microglia and does not induce major off-target effects on other cell populations of the brain parenchyma.

However, one possible limitation of the model presented here and before (Schalbetter et al., 2022) is that it requires stereotaxic surgery to induce transient microglia depletion, and thus, it causes local tissue damage at the site of the intracerebral injection. To control for possible confounds resulting from local tissue damage, we included additional cohorts of sham control mice, which underwent the same experimental manipulations as PBS controls (including anesthesia, fixation in the stereotaxic frame, and longitudinal skin incision), except that they did not receive any intracerebral injection. We found that sham controls did not differ from PBS controls with regard to the densities of microglia, neurons, or astrocytes. Moreover, sham and PBS control mice did not differ in terms of their behavioral and cognitive performance throughout all tests of interest. On the basis of these findings, we conclude that the local tissue damage caused by the intracerebral injection did not confound the identified effects of CDS-induced microglia depletion, implying furthermore that the synaptic and cognitive changes emerging after transient prefrontal microglia depletion cannot be accounted for by the stereotaxic injection itself.

We acknowledge a number of limitations in our study. First, we did not ascertain causal relationships between synaptic and cognitive measures in our model, so that the precise neuronal substrates of the observed cognitive deficits remain elusive. Second, we did not explore whether the structural synaptic deficits are accompanied by functional changes in prefrontal neurons. Based on our previous electrophysiological studies conducted in the male microglia depletion model (Schalbetter et al., 2022), however, we deem it very likely that the synaptic deficits in females would be similarly associated with some degree of electrophysiological anomalies. Third, even though our findings support the hypothesis that prefrontal microglia deficiency leads to lasting synaptic changes in the adult PFC, our study did not assess the temporal dynamics of this association. Therefore, additional longitudinal or cross-sectional investigations examining cognitive functions and synaptic structures at successive stages of adolescent-to-adult maturation will be required in future studies.

Notwithstanding these limitations, we conclude that microglia contribute to the maturation of the female PFC in a similar way to prefrontal maturation occurring in males, such that a cell-specific and temporary deficiency of prefrontal microglia restricted to adolescence is sufficient to cause lasting synaptic and cognitive impairments in adulthood. The experimental model system described here and before (Schalbetter et al., 2022) offers unique opportunities to investigate the pathophysiological relevance of impaired microglial functions in neurodevelopmental disorders, especially those that involve structural and functional deficits in the PFC. With its establishment in female mice, the

model now allows experimental investigations of this kind with regards to both male and female subjects. In a broader context, the present findings corroborate the hypothesis that microglial deficiency is likely to be etiologically relevant for some neurodevelopmental conditions and psychiatric disorders (Block et al., 2022; Bolton et al., 2022; Hayes et al., 2022, Smith et al., 2022), especially for those that have their full onset in late adolescence or early adulthood.

Declaration of Competing Interest

Unrelated to the current article, UM has received financial support from Boehringer Ingelheim, Wren Therapeutics, and Takeda Pharmaceutical Company. All authors declare that they have no competing financial interests or personal relationships that could have appeared to influence the work reported in this paper.

Data availability

Data will be made available on request.

Acknowledgements

The present study was financially supported by the Swiss National Science Foundation, Switzerland (grant No. 310030_188524 and 407940_206399 awarded to U.M.; grant No. PZ00P3_202149 awarded to T.N.). Additional financial support was received by a “Postdoc-Forschungskredit” grant (FK-22-065) awarded to S.M.S by the University of Zurich (UZH), Switzerland.

Appendix A. Supplementary data

Supplementary data to this article can be found online at https://doi.org/10.1016/j.bbi.2023.04.007.

References

Barker, G.R.I., Bird, F., Alexander, V., Warburton, E.C., 2007. Recognition memory for objects, place, and temporal order: A disconnection analysis of the role of the medial prefrontal cortex and perirhinal cortex. J. Neurosci. 27 (11), 2948–2957.
Belzung, C., Griebel, G., 2001. Measuring normal and pathological anxiety-like behaviour in mice: a review. Behav. Brain Res. 125 (1-2), 141–149.
Berry, K.P., Nedivi, E., 2017. Spine dynamics: Are they all the same? Neuron 96 (1), 43–55.
Bicks, L.K., Koike, H., Akbarian, S., Morishita, H., 2015. Prefrontal cortex and social cognition in mouse and man. Front. Psychol. 6, 1805.
Block, C.L., Eroglu, O., Mague, S.D., Smith, C.J., Ceasrine, A.M., Sriworarat, C., Blount, C., Beben, K.A., Malacon, K.E., Ndubuizu, N., Talbot, A., Gallagher, N.M., Chan Jo, Y., Nyangacha, T., Carlson, D.E., Dzirasa, K., Eroglu, C., Bilbo, S.D., 2022. Prenatal environmental stressors impair postnatal microglia function and adult behavior in males. Cell Rep. 40 (5).
Bolton, J.L., Short, A.K., Othy, S., Kooiker, C.L., Shao, M., Gunn, B.G., Beck, J., Bai, X., Law, S.M., Savage, J.C., Lambert, J.J., Belelli, D., Tremblay, M.-È., Cahalan, M.D., Baram, T.Z., 2022. Early stress-induced impaired microglial pruning of excitatory synapses on immature CRH-expressing neurons provokes aberrant adult stress responses. Cell Rep. 38 (13).
Caballero, A., Granberg, R., Tseng, K.Y., 2016. Mechanisms contributing to prefrontal cortex maturation during adolescence. Neurosci. Biobehav. Rev. 70, 4–12.
Carlén, M., 2017. What constitutes the prefrontal cortex? Science 358 (6362), 478–482.
Chai, Y.a., Chimelis-Santiago, J.R., Bixler, K.A., Aalsma, M., Yu, M., Hulvershorn, L.A., 2021. Sex-specific frontal-striatal connectivity differences among adolescents with externalizing disorders. Neuroimage Clin. 32.
Cheadle, L., Rivera, S.A., Phelps, J.S., Ennis, K.A., Stevens, B., Burkly, L.C., Lee, W.-C., Greenberg, M.E., 2020. Sensory experience engages microglia to shape neural connectivity through a non-phagocytic mechanism. Neuron 108 (3), 451–468.e9.
Chini, M., Hanganu-Opatz, I.L., 2021. Prefrontal cortex development in health and disease: Lessons from rodents and humans. Trends Neurosci. 44 (3), 227–240.
Choii, G., Ko, J., 2015. Gephyrin: A central GABAergic synapse organizer. Exp. Mol. Med. 47, e158.
Delatour, B., Gisquet-Verrier, P., 2001. Involvement of the dorsal anterior cingulate cortex in temporal behavioral sequencing: subregional analysis of the medial prefrontal cortex in rat. Behav. Brain Res. 126, 105–114.
Drzewiecki, C.M., Willing, J., Juraska, J.M., 2016. Synaptic number changes in the medial prefrontal cortex across adolescence in male and female rats: A role for pubertal onset. Synapse 70 (9), 361–368.
Elmore, M.P., Najafi, A., Koike, M., Dagher, N., Spangenberg, E., Rice, R., Kitazawa, M., Matusow, B., Nguyen, H., West, B., Green, K., 2014. Colony-stimulating factor 1 receptor signaling is necessary for microglia viability, unmasking a microglia progenitor cell in the adult brain. Neuron 82 (2), 380–397.
Falk, E.N., Norman, K.J., Garkun, Y., Demars, M.P., Im, S., Taccheri, G., Short, J., Caro, K., McCraney, S.E., Cho, C., Smith, M.R., Lin, H.M., Koike, H., Bateh, J., Maccario, P., Waltrip, L., Janis, M., Morishita, H., 2021. Nicotinic regulation of local and long-range input balance drives top-down attentional circuit maturation. Sci. Adv. 7 (10), eabe1527.
Ferrer-Quintero, M., Fernández, D., López-Carrilero, R., Birulés, I., Barajas, A., Lorente-Rovira, E., Luengo, A., Díaz-Cutraro, L., Verdaguer, M., García-Mieres, H., et al., 2022. Males and females with first episode psychosis present distinct profiles of social cognition and metacognition. Eur. Arch. Psychiatry Clin. Neurosci. 272, 1169–1181.
Ginhoux, F., Greter, M., Leboeuf, M., Nandi, S., See, P., Gokhan, S., Mehler, M.F., Conway, S.J., Ng, L.G., Stanley, E.R., Samokhvalov, I.M., Merad, M., 2010. Fate mapping analysis reveals that adult microglia derive from primitive macrophages. Science 330 (6005), 841–845.
Gogtay, N., Giedd, J.N., Lusk, L., Hayashi, K.M., Greenstein, D., Vaituzis, A.C., Nugent, T. F., Herman, D.H., Clasen, L.S., Toga, A.W., Rapoport, J.L., Thompson, P.M., 2004. Dynamic mapping of human cortical development during childhood through early adulthood. PNAS 101 (21), 8174–8179.
Guneykaya, D., Ivanov, A., Hernandez, D.P., Haage, V., Wojtas, B., Meyer, N., Maricos, M., Jordan, P., Buonfiglioli, A., Gielniewski, B., Ochocka, N., Cömert, C., Friedrich, C., Artiles, L.S., Kaminska, B., Mertins, P., Beule, D., Kettenmann, H., Wolf, S.A., 2018. Transcriptional and translational differences of microglia from male and female brains. Cell Rep. 24 (10), 2773–2783.e6.
Han, X., Li, Q., Lan, X.i., EL-Mufti, L., Ren, H., Wang, J., 2019. Microglial depletion with clodronate liposomes increases proinflammatory cytokine levels, induces astrocyte activation, and damages blood vessel integrity. Mol. Neurobiol. 56 (9), 6184–6196.
Hanamsagar, R., Alter, M.D., Block, C.S., Sullivan, H., Bolton, J.L., Bilbo, S.D., 2017. Generation of a microglial developmental index in mice and in humans reveals a sex difference in maturation and immune reactivity. Glia 65 (9), 1504–1520.
Hannesson, D.K., Vacca, G., Howland, J.G., Phillips, A.G., 2004. Medial prefrontal cortex is involved in spatial temporal order memory but not spatial recognition memory in tests relying on spontaneous exploration in rats. Behav. Brain Res. 153 (1), 273–285.
Harrison, P.J., Colbourne, L., Harrison, C.H., 2020. The neuropathology of bipolar disorder: Systematic review and meta-analysis. Mol. Psychiatry 25 (8), 1787–1808.
Hayes, L.N., An, K., Carloni, E., Li, F., Vincent, E., Trippaers, C., Paranjpe, M., Dölen, G., Goff, L.A., Ramos, A., Kano, S.-I., Sawa, A., 2022. Prenatal immune stress blunts microglia reactivity, impairing neurocircuitry. Nature 610 (7931), 327–334.
Hong, S., Dissing-Olesen, L., Stevens, B., 2016. New insights on the role of microglia in synaptic pruning in health and disease. Curr. Opin. Neurobiol. 36, 128–134.
Huang, Y., Xu, Z., Xiong, S., Sun, F., Qin, G., Hu, G., Wang, J., Zhao, L., Liang, Y.-X., Wu, T., Lu, Z., Humayun, M.S., So, K.-F., Pan, Y., Li, N., Yuan, T.-F., Rao, Y., Peng, B. o., 2018. Repopulated microglia are solely derived from the proliferation of residual microglia after acute depletion. Nat. Neurosci. 21 (4), 530–540.
Jacobs, A.J., Castillo-Ruiz, A., Cisternas, C.D., Forger, N.G., 2019. Microglial depletion causes region-specific changes to developmental neuronal cell death in the mouse brain. Dev. Neurobiol. 79 (8), 769–779.
Jay, T.R., von Saucken, V.E., Muñoz, B., Codocedo, J.F., Atwood, B.K., Lamb, B.T., Landreth, G.E., 2019. TREM2 is required for microglial instruction of astrocytic synaptic engulfment in neurodevelopment. Glia 67, 1873–1892.
Kierdorf, K., Erny, D., Goldmann, T., Sander, V., Schulz, C., Perdiguero, E.G., Wieghofer, P., Heinrich, A., Riemke, P., Hölscher, C., Müller, D.N., Luckow, B., Brocker, T., Debowski, K., Fritz, G., Opdenakker, G., Diefenbach, A., Biber, K., Heikenwalder, M., Geissmann, F., Rosenbauer, F., Prinz, M., 2013. Microglia emerge from erythromyeloid precursors via Pu.1- and Irf8-dependent pathways. Nat. Neurosci. 16 (3), 273–280.
Koechlin, E., Ody, C., Kouneiher, F., 2003. The architecture of cognitive control in the human prefrontal cortex. Science 302, 1181–1185.
Konishi, H., Okamoto, T., Hara, Y., Komine, O., Tamada, H., Maeda, M., Osako, F., Kobayashi, M., Nishiyama, A., Kataoka, Y., Takai, T., Udagawa, N., Jung, S., Ozato, K., Tamura, T., Tsuda, M., Yamanaka, K., Ogi, T., Sato, K., Kiyama, H., 2020. Astrocytic phagocytosis is a compensatory mechanism for microglial dysfunction. EMBO J. 39, e104464.
Koss, W.A., Belden, C.E., Hristov, A.D., Juraska, J.M., 2014. Dendritic remodeling in the adolescent medial prefrontal cortex and the basolateral amygdala of male and female rats. Synapse 68, 61–72.
Kumamaru, H., Saiwai, H., Kobayakawa, K., Kubota, K., van Rooijen, N., Inoue, K., Iwamoto, Y., Okada, S., 2012. Liposomal clodronate selectively eliminates microglia from primary astrocyte cultures. J. Neuroinflammation 9, 116.
Labouesse, M.A., Langhans, W., Meyer, U., 2015. Abnormal context–reward associations in an immune-mediated neurodevelopmental mouse model with relevance to schizophrenia. Transl. Psychiatry 5, e637.
Larsen, B., Luna, B., 2018. Adolescence as a neurobiological critical period for the development of higher-order cognition. Neurosci. Biobehav. Rev. 94, 179–195.
Le Merre, P., Ährlund-Richter, S., Carlén, M., 2021. The mouse prefrontal cortex: unity in diversity. Neuron 109, 1925–1944.
Lebrón, K., Milad, M.R., Quirk, G.J., 2004. Delayed recall of fear extinction in rats with lesions of ventral medial prefrontal cortex. Learn. Mem. 11, 544–548.
Lehenkari, P.P., Kellinsalmi, M., Näpänkangas, J.P., Ylitalo, K.V., Mönkkönen, J., Rogers, M.J., Azhayev, A., Väänänen, H.K., Hassinen, I.E., 2002. Further insight into mechanism of action of clodronate: Inhibition of mitochondrial ADP/ATP translocase by a nonhydrolyzable, adenine-containing metabolite. Mol. Pharmacol. 61, 1255–1262.

Livak, K.J., Schmittgen, T.D., 2001. Analysis of relative gene expression data using real-time quantitative PCR and the 2(-Delta Delta C(T)) method. Methods 25, 402–408.
Maren, S., Phan, K.L., Liberzon, I., 2013. The contextual brain: Implications for fear conditioning, extinction and psychopathology. Nat. Rev. Neurosci. 14, 417–428.
T. Masuda L. Amann R. Sankowski O. Staszewski M. Lenz D. Errico P., Snaidero, N., Costa Jordão, M.J., Böttcher, C., Kierdorf, K., Jung, S., Priller, J., Misgeld, T., Vlachos, A., Meyer-Luehmann, M., Knobeloch, K.P., Prinz, M., Novel Hexb-based tools for studying microglia in the CNS Nat. Immunol. 21 2020 802 815.
Mattei, D., Ivanov, A., van Oostrum, M., Pantelyushin, S., Richetto, J., Mueller, F., Beffinger, M., Schellhammer, L., Vom Berg, J., Wollscheid, B., Beule, D., Paolicelli, R.C., Meyer, U., 2020. Enzymatic dissociation induces transcriptional and proteotype bias in brain cell populations. Int. J. Mol. Sci. 21 (21), 7944.
Morgan, M.A., LeDoux, J.E., 1995. Differential contribution of dorsal and ventral medial prefrontal cortex to the acquisition and extinction of conditioned fear in rats. Behav. Neurosci. 109, 681–688.
Morgan, M.A., LeDoux, J.E., 1999. Contribution of ventrolateral prefrontal cortex to the acquisition and extinction of conditioned fear in rats. Neurobiol. Learn. Mem. 72, 244–251.
Mueller, F.S., Scarborough, J., Schalbetter, S.M., Richetto, J., Kim, E., Couch, A., Yee, Y., Lerch, J.P., Vernon, A.C., Weber-Stadlbauer, U., Meyer, U., 2021. Behavioral, neuroanatomical, and molecular correlates of resilience and susceptibility to maternal immune activation. Mol. Psychiatry 26, 396–410.
Nabel, E.M., Garkun, Y., Koike, H., Sadahiro, M., Liang, A., Norman, K.J., Taccheri, G., Demars, M.P., Im, S., Caro, K., Lopez, S., Bateh, J., Hof, P.R., Clem, R.L., Morishita, H., 2020. Adolescent frontal top-down neurons receive heightened local drive to establish adult attentional behavior in mice. Nat. Commun. 11 (1), 3983.
Nguyen, P.T., Dorman, L.C., Pan, S., Vainchtein, I.D., Han, R.T., Nakao-Inoue, H., Taloma, S.E., Barron, J.J., Molofsky, A.B., Kheirbek, M.A., Molofsky, A.V., 2020. Microglial remodeling of the extracellular matrix promotes synapse plasticity. Cell 182, 388–403.
Notter, T., Panzanelli, P., Pfister, S., Mircsof, D., Fritschy, J.M., 2014. A protocol for concurrent high-quality immunohistochemical and biochemical analyses in adult mouse central nervous system. Eur. J. Neurosci. 39, 165–175.
Notter, T., Coughlin, J.M., Gschwind, T., Weber-Stadlbauer, U., Wang, Y., Kassiou, M., Vernon, A.C., Benke, D., Pomper, M.G., Sawa, A., Meyer, U., 2018. Translational evaluation of translocator protein as a marker of neuroinflammation in schizophrenia. Mol. Psychiatry 23, 323–334.
Notter, T., Schalbetter, S.M., Clifton, N.E., Mattei, D., Richetto, J., Thomas, K., Meyer, U., Hall, J., 2021. Neuronal activity increases translocator protein (TSPO) levels. Mol. Psychiatry 26, 2025–2037.
Paolicelli, R.C., Sierra, A., Stevens, B., Tremblay, M.E., Aguzzi, A., Ajami, B., Amit, I., Audinat, E., Bechmann, I., Bennett, M., et al., 2022. Microglia states and nomenclature: A field at its crossroads. Neuron 110, 3458–3483.
Parkhurst, C.N., Yang, G., Ninan, I., Savas, J.N., Yates 3rd, J.R., Lafaille, J.J., Hempstead, B.L., Littman, D.R., Gan, W.B., 2013. Microglia promote learning-dependent synapse formation through brain-derived neurotrophic factor. Cell 155, 1596–1609.
Richetto, J., Labouesse, M.A., Poe, M.M., Cook, J.M., Grace, A.A., Riva, M.A., Meyer, U., 2015. Behavioral effects of the benzodiazepine-positive allosteric modulator SH-053-2'F-S-CH_3 in an immune-mediated neurodevelopmental disruption model. Int. J. Neuropsychopharmacol. 18, pyu055.
Riecher-Rössler, A., 2017. Oestrogens, prolactin, hypothalamic-pituitary-gonadal axis, and schizophrenic psychoses. Lancet Psychiatry 4, 63–72.
Sakurai, T., Gamo, N.J., Hikida, T., Kim, S.H., Murai, T., Tomoda, T., Sawa, A., 2015. Converging models of schizophrenia – Network alterations of prefrontal cortex underlying cognitive impairments. Prog. Neurobiol. 134, 178–201.
Schafer, D.P., Lehrman, E.K., Kautzman, A.G., Koyama, R., Mardinly, A.R., Yamasaki, R., Ransohoff, R.M., Greenberg, M.E., Barres, B.A., Stevens, B., 2012. Microglia sculpt postnatal neural circuits in an activity and complement-dependent manner. Neuron 74, 691–705.
Schalbetter, S.M., Mueller, F.S., Scarborough, J., Richetto, J., Weber-Stadlbauer, U., Meyer, U., Notter, T., 2021. Oral application of clozapine-N-oxide using the micropipette-guided drug administration (MDA) method in mouse DREADD systems. Lab Anim. (NY) 50, 69–75.
Schalbetter, S.M., von Arx, A.S., Cruz-Ochoa, N., Dawson, K., Ivanov, A., Mueller, F.S., Lin, H.Y., Amport, R., Mildenberger, W., Mattei, D., Beule, D., Földy, C., Greter, M., Notter, T., Meyer, U., 2022. Adolescence is a sensitive period for prefrontal microglia to act on cognitive development. Sci. Adv. 8, eabi6672.
Schwarz, M., Bilbo, S.D., 2012. Sex, glia, and development: interactions in health and disease. Horm. Behav. 62, 243–253.
Selemon, L.D., Zecevic, N., 2015. Schizophrenia: A tale of two critical periods for prefrontal cortical development. Transl. Psychiatry 5, e623.
Sierra-Mercado, D., Padilla-Coreano, N., Quirk, G.J., 2011. Dissociable roles of prelimbic and infralimbic cortices, ventral hippocampus, and basolateral amygdala in the expression and extinction of conditioned fear. Neuropsychopharmacology 36, 529–538.
Smith, C.J., Lintz, T., Clark, M.J., Malacon, K.E., Abiad, A., Constantino, N.J., Kim, V.J., Jo, Y.C., Alonso-Caraballo, Y., Bilbo, S.D., Chartoff, E.H., 2022. Prenatal opioid exposure inhibits microglial sculpting of the dopamine system selectively in adolescent male offspring. Neuropsychopharmacology 47, 1755–1763.
Sotres-Bayon, F., Cain, C.K., LeDoux, J.E., 2006. Brain mechanisms of fear extinction: historical perspectives on the contribution of prefrontal cortex. Biol. Psychiatry 60, 329–336.
Torres, L., Danver, J., Ji, K., Miyauchi, J.T., Chen, D., Anderson, M.E., West, B.L., Robinson, J.K., Tsirka, S.E., 2016. Dynamic microglial modulation of spatial learning and social behavior. Brain Behav. Immun. 55, 6–16.
VanRyzin, J.W., Marquardt, A.E., Argue, K.J., Vecchiarelli, H.A., Ashton, S.E., Arambula, S.E., Hill, M.N., McCarthy, M.M., 2019. Microglial phagocytosis of newborn cells is induced by endocannabinoids and sculpts sex differences in juvenile rat social play. Neuron 102, 435–449.
Weber-Stadlbauer, U., Richetto, J., Labouesse, M.A., Bohacek, J., Mansuy, I.M., Meyer, U., 2017. Transgenerational transmission and modification of pathological traits induced by prenatal immune activation. Mol. Psychiatry 22, 102–112.
Wolf, S.A., Boddeke, H.W., Kettenmann, H., 2017. Microglia in physiology and disease. Annu. Rev. Physiol. 79, 619–643.